Heliyon 11 (2025) e42263

Contents lists available at ScienceDirect

Heliyon

journal homepage: www.cell.com/heliyon

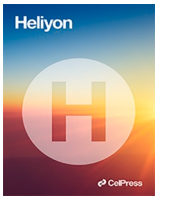

Research article

Study of different thermal management systems for traction batteries to obtain vehicle lightweighting

Giulia Sandrini *, Daniel Chindamo, Marco Gadola, Andrea Candela, Paolo Magri

Department of Mechanical and Industrial Engineering, University of Brescia, I-25123, Brescia, Italy

ARTICLE INFO

Keywords:
Vehicle lightweighting
Secondary lightweighting
Traction battery thermal management system
Energy consumption
Electric vehicle
PCM (phase change material)

ABSTRACT

Nowadays environmental sustainability is a hot topic, especially with regards to the transportation sector. In fact, political strategies are oriented to the transition towards the cleaner technologies to reduce polluting and climate-altering emissions. However, even fully electric vehicles are not characterized by zero global emissions, due to the production of electricity from sources that are not always renewable. Moreover, this type of vehicle is afflicted by the limited range provided by the battery pack and its long recharging time. So, it is useful to reduce the energy consumption through appropriate strategies, for example by means of the vehicle lightweighting. In this paper we focus on the battery pack lightweighting by considering different passive battery cooling systems as a replacement for the standard active one. The passive systems considered are air and PCM-based (Phase Change Material) cooling systems. In addition to the primary lightweighting given by the replacement of the cooling system, the secondary lightweighting obtained by reducing the capacity of the battery pack to return to the range of the starting reference vehicle has been also considered. Three tools were used for the study: VI-CarRealTime and another consolidate vehicle model to obtain the power demand on a standard driving cycle; and an ad-hoc battery system model, configurable according to the cooling system. The simulations showed that the air-cooled system leads to greater lightweighting, but it makes the battery cells work far from 20 °C (optimal operating temperature) and therefore it could lead to greater battery cell degradation and its field of application must be limited to vehicles operating in fleets, with predictable mission; this can be overcome by using an appropriate PCM-based cooling system, stearyl alcohol. Furthermore, using a PCM, glycerol, with a melting point close to the optimal operating temperature of the batteries, allows to reduce the cell degradation.

1. Introduction

Nowadays environmental sustainability is a hot topic, especially with regards to the transportation sector. In fact, most of the local, national, and international regulations are increasingly pushing towards mobility with zero local environmental impacts and therefore towards the electrification of the circulating fleet. In this regard it is appropriate to cite the ordinary legislative procedure 2021/0197 (COD) [1].

* Corresponding author.
E-mail addresses: giulia.sandrini@unibs.it (G. Sandrini), daniel.chindamo@unibs.it (D. Chindamo), marco.gadola@unibs.it (M. Gadola), andrea.candela@unibs.it (A. Candela), p.magri003@unibs.it (P. Magri).

https://doi.org/10.1016/j.heliyon.2025.e42263
Received 8 July 2024; Received in revised form 22 January 2025; Accepted 23 January 2025
Available online 27 January 2025

However, even full electric vehicles can't achieve zero global emissions, mainly due to the production of electricity from sources that are not always renewable. Furthermore, a major limitation that afflicts this type of vehicle is the limited range provided by the battery pack and its long recharging time, when compared with the refuelling times of traditional internal combustion engine vehicles (diesel and petrol vehicles). To mitigate the two defects mentioned, it would be very useful to reduce the energy consumption of these vehicles. This can be achieved in various ways, such as optimizing energy management on board the vehicle through appropriate regenerative braking logic [2,3]. However, an interesting alternative concerns the vehicle lightweighting [4–6].

The topic of vehicle lightweighting is much debated today, in fact, a significant number of research programs have funded and continue to fund various projects on this topic. For example, the Natural Resources Canada funded [7] (year 2021, the Program of Energy Research and Development, PERD), and [8] (year 2023); the U.S. Navy's Office of Naval Research sponsored the ALMMII (American Lightweight Materials Manufacturing Innovation Institute), which funded the paper [5] (2019); and the U.S. Department of Energy sponsored the project reported in Ref. [9] (2016). Furthermore, the Tucana research project [10], led by Jaguar Land Rover (JLR), with the collaboration of experts from WMG (Warwick Manufacturing Group) at the University of Warwick, focuses on lightweighting technology to develop stiffer and lighter vehicle structures. Finally, in Italy, the MOST project (National Center for Sustainable Mobility) [11] aims to implement modern, sustainable, and inclusive solutions across the national territory, in collaboration with 24 universities, the CNR (National Research Council), and 24 major companies. Among the universities involved there is also the University of Brescia, which works on vehicle lightweighting from the point of view of the results obtained, in relation to energy consumption, environmental factors and the improvement of the active safety of the vehicle.

There are different lightweighting methods, which are divided into primary and secondary lightweighting. Regarding the primary, several studies are referred to the strategy of material substitution and mass reduction [7,12], in particular [7] considers different alloy and technologies of components manufacturing [13], studies the use of plastic materials to obtain lightweighting. Some other studies analyse the benefits of lightweighting in terms of environmental impacts, for example from an LCA (Life Cycle Assessment) perspective or considering greenhouse gas emissions [14–21]. Other papers consider specific indices for evaluating the outcome of the lightweighting. Some studies use the FRV (Fuel Reduction Value) index, expressed in L/(100 km · 100 kg) [16–21], others use an index more suitable for electric vehicles, the ERV (Energy Reduction Value) index, expressed in kWh/(100 km · 100 kg) [16,22–24]. One of the most interesting is [16] which uses FRV index for internal combustion engine lightweighting evaluation, while it uses the ERV coefficient for electric vehicles. On the other hand, the secondary effects of lightweighting concern -among the others-the downsizing of the powertrain, transmission, and battery pack [6]. The secondary lightweighting effects are evaluated in many studies, such as [17, 20,21].

As the battery pack is among the components of a full electric vehicles associated with the highest environmental impact [25], this study investigates the possibility of lightweighting the battery pack.

Replacing the cooling system in a battery pack with a lightweight alternative can substantially enhance the overall efficiency and performance of electric vehicles. Numerous studies have investigated various lightweight liquid cooling solutions and their effects on battery thermal management systems [26–29]. However, these studies mainly consist in the optimization of the thermal conditioning system, its management, its design and its structure, so that the latter can be lighter than its non-optimized configuration.

Conversely, in this study, the lightweighting of the battery pack is achieved by replacing the standard active liquid-cooling system with a simpler (and hance lighter) passive system such as air-cooling system or PCM-based cooling system. The use of PCMs (Phase Change Materials) for the construction of cooling systems for battery packs of electric vehicles can in fact be found in several studies present in the scientific literature [30–34].

The possibility of further lightweighting the vehicle (secondary) will also be evaluated; this will be done by re-establishing the initial range of the vehicle through cell number reduction as it increased after the primary lightweight (lighter vehicle requires less energy). For the purpose of this study a baseline vehicle with an active cooling system has been used and compared with a set of equivalent vehicles equipped with passive cooling systems, in particular an air-cooling system and two different PCM-based (Phase Change Material) cooling systems. As it will be seen in this paper, some of the cooling systems considered can only be used for vehicles with a known mission, such as operating in fleets, while others can also be used for general purpose vehicles. Finally, conclusion remarks will be given at the end of this paper, discussing the feasibility of replacing a standard and optimal battery liquid-cooling system with a lighter passive cooling system; some limiting factors will be also discussed, such as the greater cells degradation when using a passive air-cooling system.

The work presented in this scientific paper is partially summarized in the conference paper [35].

2. Material and methods

For the purpose of this study, the baseline vehicle used was the electric vehicle "SedanCar_FullElectric" included in the VI-CarRealTime (VI-CRT) simulation package. VI-CRT is a vehicle dynamics simulation tool developed by VI-Grade, and it is widely considered the reference in the automotive field [36,37]. Furthermore, we chose the WLTP procedure (Worldwide Harmonized Light-Duty Vehicles Test Procedure) [38] as the reference mission, therefore the driving cycle considered in this study was the WLTC (Worldwide Harmonized Light-Duty Vehicles Test Cycle), class 3b (see Figure B1).

By means of VI-CRT simulation tool, the torque and angular speeds time histories of each electric motors on the WLTC driving cycle have been calculated (the vehicle chosen is in fact all-wheel drive, with a motor for each axle). These values have been then used as inputs for the simulation tool described in Ref. [39], the TEST model (Target-speed EV, Electric Vehicle, Simulation Tool) with the integrations reported in Refs. [2,3,23,40–42], to obtain the power required from the battery pack on the above-mentioned driving cycle. Finally, a battery pack model has been built; this was needed to study the effect of each cooling system in terms of thermal

management, battery pack temperature, battery State of Charge (SOC) sensitivity and other parameters described later. The thermally managed battery pack model is simplified, as the goal of this work is a feasibility study rather than precise thermal management modelling.

The operational steps adopted in this study, for each vehicle equipped with each cooling system (active and passive), are summarized below.

1. VI-CarRealTime (VI-CRT) simulations to obtain the torque and angular speeds time histories of each electric motors on the WLTC driving cycle.
2. Use of an energy consumption simulation tool (TEST model) to obtain the power required from the battery pack starting from motor torque and angular speed inputs.
3. Simulations using a battery model (with thermal management) specifically designed for this study, to analyse the effect of each cooling system (battery pack temperature, SOC, etc.).

In particular.

1. VI-CarRealTime is a well-established software and version 19 of it was used for the study.
2. The TEST model is a consolidated tool and already widely used by our research group, as demonstrated in the studies [2,3,35,24,39–42]. This model is therefore already available to our group, for this study it was only necessary to perform an integration to the model, to allow it to receive motor torque and speed as input, instead of the vehicle speed profile.
3. The battery pack model used is the "Datasheet Battery" of the Simulink library, while its thermal management model was reconstructed in Simulink using the information contained in Refs. [43,44]. The overall model given by the battery pack and its thermal conditioning system is therefore extremely simplified, and therefore appropriate for the feasibility study under consideration.

2.1. Vehicle model

This section describes the "SedanCar_FullElectric" coming from VI-CarRealTime libriaries. It is a four-wheel drive vehicle, equipped with an electric motor for each axle, used as the baseline vehicle for the purpose of this study.

Please note that for the sake of simplicity and to better highlight the effect of the cooling system on the battery thermal management, the regenerative braking has been deactivated. Fig. 1 reports the motor torque characteristics of the two motors equipped in the SedanCar, while Table 1 shows the main vehicle data.

The power absorbed by the auxiliaries is estimated in 1500 W [2], including the consumption of the battery pack thermal management system.

2.2. VI-CarRealTime simulations

The baseline vehicle model used for this study can be considered fully validated and highly representative of a real vehicle, as the VI-CarRealTime documentation states that all VI system data either come from experimental tests performed on track or in a laboratory

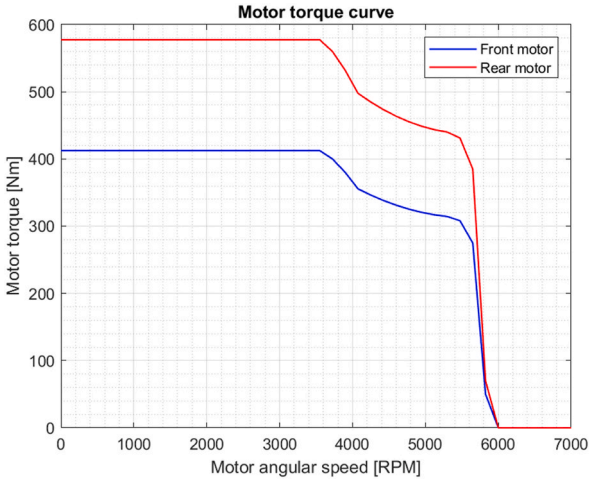

Fig. 1. Motor torque curve. Motor torque characteristics of the front and rear electric motors of the "SedanCar_FullElectric" of VI-CarRealTime software vehicle library.

Table 1
Main vehicle data of the "SedanCar_FullElectric of VI-CarRealTime, with some additional information regarding the electrical efficiency and some other useful data for TEST [39] simulations.

	Parameter	Value	Unit
VI-CarRealTime parameters	Total mass of the vehicle (with the driver)	1986.6[b]	kg
	Frontal area	2	m^2
	Drag coefficient	0.8698	–
	Downforce coefficient (WHF)[a]	−0.0613	m^2
	Wheel radius (front and rear)	0.317	m
	Rolling friction coefficient	0.01	–
	Moment of inertia of the wheels (front and rear)	1.389150	$kg•m^2$
	Front motor reductor transmission ratio	1	–
	Rear motor reductor transmission ratio	1	–
	Transmission ratio of the front differential	3.65	–
	Transmission ratio of the rear differential	3.75	
	Moment of inertia of the motors (front and rear)	0.001	$kg•m^2$
	Moment of inertia of the rotating components of the front transmission	0.0001	$kg•m^2$
	Moment of inertia of the rotating components of the rear transmission	0.0002	$kg•m^2$
TEST parameters	Distribution of motor torque to the front in acceleration and in braking	0.42	–
	Motor electrical efficiency (front and rear)	0.98	–
	Transmission efficiency (front and rear)	0.95	–
	Power absorbed by the vehicle accessories	1500[b]	W
	Electrical connection cable resistivity	$1.7•10^{-8}$	Ω•m
	Length of the electrical connection cable of the front traction	3	m
	Section area of the electrical cable of the front traction	$1.2•10^{-4}$	m^2
	Length of the electrical connection cable of the rear traction	3	m
	Section area of the electrical cable of the rear traction	$1.2•10^{-4}$	m^2
	Inverter efficiency in charge	0.8	–
	Inverter efficiency in discharge	0.8	–

[a] For more information see equation (2) of [41].
[b] Default value: value relative to the reference vehicle; this value is modified for some simulations of the study.

or from a virtual test performed within Adams Car [45].

Fig. 2 shows the results, in terms of motor torque (Fig. 2a) and angular speed (Fig. 2b) of each electric motor of the reference Sedan Car, as a result of the simulation performed with VI-CRT on the WLTC driving cycle (class 3b).

Depending on the cooling system configuration used, simulations have been repeated with different vehicle mass as function of the lightweighting achieved.

2.3. TEST model simulations

The TEST model (Target-speed EV Simulation Tool) described in Ref. [39], with the modifications and integrations described in Refs. [2,3,23,40–42], has been used to calculate the time history of the power flowing through the battery.

The first version of the TEST model required as input the target speed profile that the vehicle must follow during the simulation. Modifications have been made to the model allowing for the calculation of the power requests (concerning both motors and battery pack) starting from the time histories of motor torque and angular speed of the motors as inputs. The original functions of the model have not been compromised, as it is possible to set, via a binary variable, one or the other type of input.

At this stage an accurate model of the battery pack is not required yet, assuming that the battery pack is able to provide the entire amount of power required from the driving cycle without limitations.

Fig. 3 shows the power demand of the baseline vehicle model on the WLTC cycle, class 3b.

2.4. Simulink model of the battery pack with thermal management

The battery pack, including its internal thermal behaviour, has been modelled using Matlab-Simulink. This model is fed using the power demand coming from the TEST model [39], as reported in the previous paragraph. This allows to separate battery simulations from the vehicle dynamics simulations (performed with VI-CRT and TEST model), making the entire simulation process quicker.

The battery pack model with internal thermal model and temperature management has been built starting from the "Datasheet Battery" [46] subsystem of the "Library Browser" in Simulink and adding its thermal model and thermal management system (cooling system) as an external part using the data found in literature [43,44,47]. In this way, starting from the simple Simulink battery model, it is possible to obtain a simplified battery pack and its thermal conditioning system assembly, characterized by quick calculation times, useful for a feasibility study. It should be remembered that the study in question does not consist of an accurate modelling of thermal management system.

2.4.1. Datasheet Battery

Below are the input parameters to be provided to the "Datasheet Battery" subsystem [46].

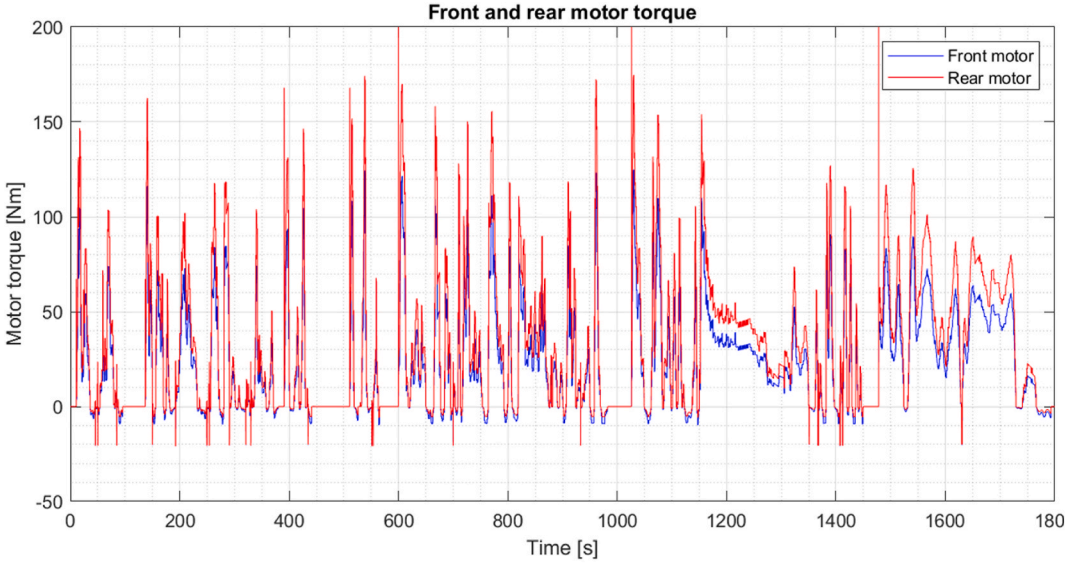

(a)

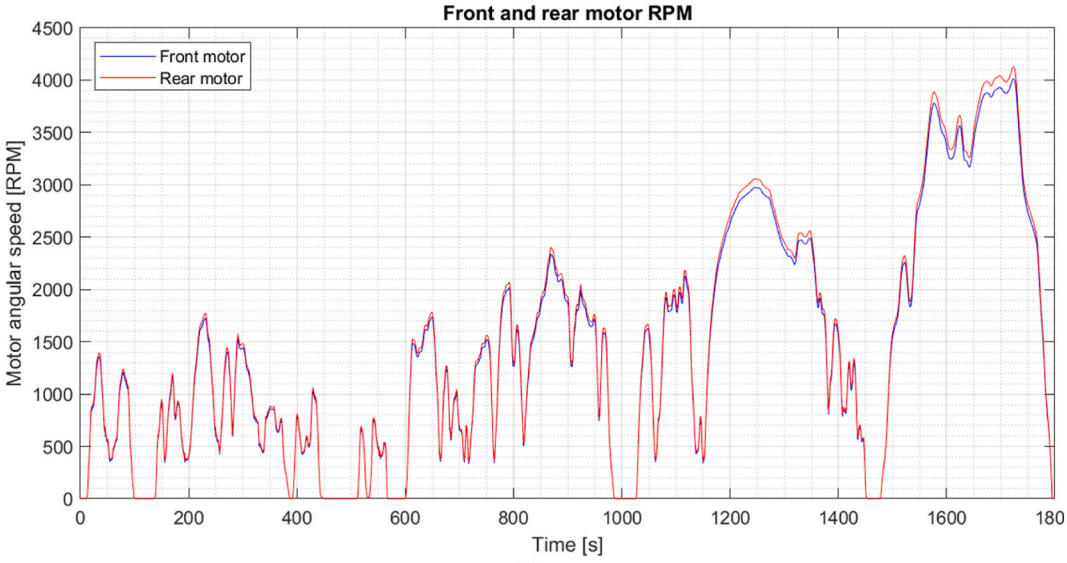

(b)

Fig. 2. Motor torque and RPM. (a) Front and rear motor torque, and (b) front and rear angular speed of the electric motors of the reference car on the WLTC (class 3b) driving cycle.

- Battery current ($I_{bat} = P_{demand}/V_{bat\_prev}$, where P_{demand} is the power demand and V_{bat_prev} is the battery pack voltage of the instant of calculation preceding the one considered);
- Temperature of the battery pack;
- Number of cells in series in the battery pack (N_s);
- Number of cells in parallel in the battery pack (N_p);
- Rated capacity of the single battery cell at nominal temperature (C_{cell});
- Open Circuit Voltage (OCV) of a single cell as a function of the battery State of Charge (SOC);
- Internal resistance of a single cell as a function of the battery SOC and of the battery temperature;
- Initial battery capacity (equal to $C_{cell} \bullet N_p \bullet SOC_{init}/100$, where SOC_{init} is the value of initial battery State of Charge at the start of the simulation, expressed in percentage).

The initial value of the battery voltage depends on the initial SOC (SOC_{init}) and it is obtained via a Simulink Lookup Table, starting from the open-circuit voltage (OCV) of the cells as a function of the SOC. The OCV value obtained by considering the initial SOC is then multiplied by the number of cells placed in series (N_s) to obtain the initial voltage of the battery pack (at the start of the simulation).

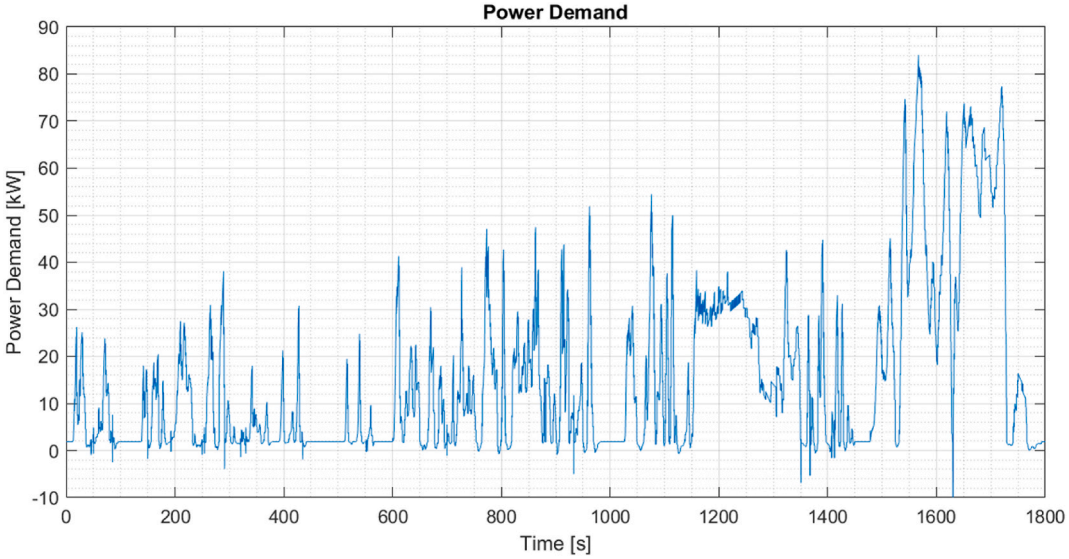

Fig. 3. Power demand. Power that the reference vehicle requires from the battery pack.

The average temperature of the cells is considered as input temperature to "Datasheet Battery", but relative to the instant of calculation preceding the one considered (T_{bat_prev}, expressed in Kelvin). T_{bat_init} is defined as the initial value at the start of the simulation and it is an input parameter.

Below are the relevant outputs provided by the "Datasheet Battery" subsystem [46].

- Battery voltage (V_{bat});
- Battery State of Charge (SOC);
- Battery network power (P_{bat});
- Battery network power loss (P_{loss});
- Energy of the single cell (C_{cell}, expressed in Ah).

In the Simulink battery model it is assumed that the single cells are ideally identical to each other (same OCV, same internal resistance, same nominal capacity), at the start of the simulation they are all in the same initial condition (same initial C_{cell}), and that during the simulation all cells remain perfectly balanced at any time (same C_{cell} between them).

2.5. Data of the battery pack and of the battery thermal management (cooling system)

In this paper, the battery pack described in Ref. [47] and considered for the studies [43,44] was used. The battery pack is made up

Table 2
Main characteristics of the battery pack of the reference vehicle of the study, with NCA-18650 cells.

Parameter	Nomenclature	Value	Unit
Initial battery State of Charge (SOC)	SOC_{init}	80[d]	%
Initial battery pack temperature	T_{bat_init}	25[d]	°C
Rated capacity of the single battery cell [a,b]	C_{cell}	2.75	Ah
Total number of cells in the battery pack [a,b]	–	5664	–
Number of cells in series in the battery pack [a]	N_s	96	–
Number of cells in parallel in the battery pack [a]	N_p	59	–
Operating temperature in charge [c]	–	0 to 45	°C
Operating temperature in discharge [c]	–	−20 to 60	°C
Average density of the battery cell [a,b]	ρ_{bat}	2841.5	$kg \bullet m^{-3}$
Specific heat capacity of the battery cell [b]	$c_{p,bat}$	1.098	$kJ \bullet kg^{-1} \bullet K^{-1}$
Volume of a single cell, average value between all the cells [a]	v_{cell}	$1.654 \bullet 10^{-5}$	m^3
Heat conductance at the cooling plate [b]	K_{CP}	1.0[d]	kW/°C
Average temperature of the refrigerant	T_{CP}	20[d]	°C

[a] Ref. [47].
[b] Ref. [43].
[c] Ref. [48].
[d] Default value: value relative to the reference vehicle; this value is modified for some simulations of the study.

of 5664 cells of the NCA-18650 type, in 96S59P configuration (96 cells in series and 59 in parallel), with a capacity of approximately 56 kWh. In Ref. [47] reference is made to the N18650CL cells, produced by Shenzhen BAK Battery Co. Ltd., with mass weight 47.0 g, internal resistance ≤35 mΩ, with NCA (nickel–cobalt–aluminium) cathode, a nominal capacity of 2.75 Ah, and a nominal voltage of 3.6 V. These are cells with the same characteristics as the Samsung-18650, model name "INR18650-29E" [48]. The main characteristics of these cells and battery pack used are described in Table 2.

Considering the charging operating temperature range of the cells between −20 and 60 °C, the optimal operating temperature can be considered equal to the average value between the two extremes of the range, therefore equal to 20 °C. It was therefore chosen to maintain the temperature of the refrigerant coming from the cooling system at a constant value of 20 °C.

The Open Circuit Voltage (OCV) of the single battery cell was obtained from Fig. 9b of [49], and it is related to a Samsung-18650 cell (see Figure B2.a). The internal resistance of the single battery cell was obtained from Fig. 5 of [50] (see Figure B2.b), and it is related to a Panasonic 18650 LIB (Lithium-Ion Battery) cell, NCA-18650 cell equivalent to Samsung-18650 cell and N18650CL cell produced by Shenzhen BAK Battery Co. Ltd.

2.5.1. Battery thermal management system weight

To estimate the weight of the thermal management system (cooling system), the battery pack was reconstructed in "BatPaC", a software developed by Argonne National Laboratory [51]. Table 3 shows the weight results of the thermal management system obtained.

Adding the mass of cooling system within the pack and the mass of cooling system exterior to the battery pack gives the total mass of the cooling system, equal to 88.84 kg.

2.5.2. PCMs (phase change materials) selection

As regards passive systems cooled by Phase Change Materials (PCMs), two particular cases were chosen to be considered.

1. a PCM with a melting point temperature close to the optimum operating temperature of the battery pack, to allow the latter to operate as close to that temperature as possible;
2. a PCM with a temperature slightly below (by a few degrees) the maximum operating temperature limit of the battery pack, in order to try to avoid overheating the pack.

Table 2 of [52] reports a list of common PCM materials suitable for the automotive sector, for battery cooling.

Considering that the battery pack has an operating range between −20 and 60 °C and an optimum operating temperature of approximately 20 °C, the following PCMs were chosen from Table 2 of [52].

1. Glycerol, with a melting point of 26 °C;
2. Stearyl alcohol, with a melting point of 57 °C.

3. Calculation

Below are the equations added to the standard "Datasheet Battery", for the definition of the thermal aspects of the battery pack. The battery heat coefficient (C_h) is calculated as in equation (1) [43,44].

$$C_h = \begin{cases} (2.04 \bullet \sigma^2 + 2.79 \bullet \sigma)/100, \sigma \leq 1 \\ (3.97 \bullet \ln \sigma + 4.83)/100, \sigma > 1 \end{cases} \quad (1)$$

where σ is equal to $P_{bat}[kW] \bullet 1\ hour/C_{kWh}[kWh]$ [43,44].

Battery power storage (C_{kWh}, expressed in kWh) is defined as $C_{bat}[Ah] \bullet V_{bat}[V]/1000$, where C_{bat} is the battery energy and it is equal to $C_{cell} \bullet N_p$.

The heat generated by the batteries ($Q_{bat}[kW]$) is calculated as $C_h \bullet P_{bat}[kW]$ [43,44].

From equation (12) of [43,44], the average battery pack temperature (T_{bat}) is obtained, as in equation (2).

Table 3
Battery thermal management weights obtained thanks to BatPaC software [51].

Parameter	Value	Unit
Total mass of empty coolant panels for the pack	53.72	kg
Total mass of coolant manifold	0.13	kg
Total mass of coolant within pack	27.99	kg
Mass of cooling system within pack[a]	81.84	kg
Mass of cooling system exterior to battery packs	7.00	kg
Total mass of the cooling system	88.84	kg

[a] Sum of total mass of empty coolant panels for the pack, total mass of coolant manifold, and total mass of coolant within pack.

$$T_{bat}[^{\circ}C] = \frac{Q_{bat}[kW] - Q_{CP}[kW]}{\rho_{bat}\left[kg/m^3\right] \bullet v_{bat}[m^3] \bullet c_{p,bat}\left[kJ/kg \bullet K\right]} \bullet dt[s] + T_{bat\_prev}[^{\circ}C] \quad (2)$$

where ρ_{bat} is the average density and $c_{p,bat}$ the specific heat capacity of the battery; v_{bat} is the total volume of the batteries, considering the only cell volume not all the battery pack ($v_{bat} = v_{cell} \bullet N_s \bullet N_p$, where v_{cell} is the volume of a single cell); and Q_{CP} is the cooling heating power of the cooling plate of the thermal management system.

Finally, the cooling heating power of the cooling plate is calculated as in equation (3) [43].

$$Q_{CP} = K_{CP} \bullet \left(T_{bat\_prev} - T_{CP}\right) \quad (3)$$

where K_{CP} is the heat conductance at the cooling plate and T_{CP} is the average temperature of the refrigerant flowing in the heat exchangers.

4. Results

In this section the results in terms of energy consumption, battery pack temperature and SOC over the driving cycle will be reported, for the three following configurations.

- Baseline vehicle with active liquid-cooling system, battery thermal management system with constant refrigerant temperature.
- Passive air-cooling system.
- Passive PCM (Phase Change Material) cooling system.

4.1. Baseline vehicle with active cooling system

This section reports the results related to a simulation using the battery model with thermal management, starting from 80 % SOC, assuming an initial battery temperature equal to 25 °C and considering the refrigerant temperature constant during the entire simulation and equal to 20 °C (see from Figs. 4–6). A temperature of 20 °C was chosen to keep the battery pack at optimal operating temperatures as 20 °C is exactly in the middle of the discharge operating range (see Section 2.5).

In particular, Fig. 4a reports the battery current and the battery voltage during the entire simulation; Fig. 4b the battery SOC and the battery energy; and Fig. 4c shows the battery temperature and the refrigerant temperature.

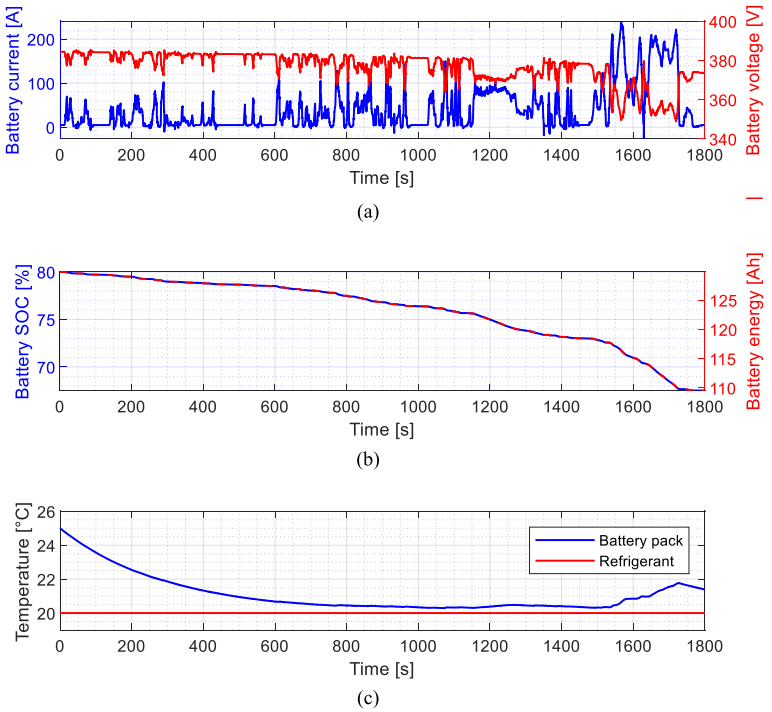

Fig. 4. Results for the baseline vehicle. Results in terms of (a) battery current and battery voltage; (b) battery SOC and battery energy; (c) battery temperature and refrigerant temperature.

As can be seen from Fig. 4c, during the simulation, the battery pack temperature tends to approach the temperature of the refrigerant, to deviate further towards the end of the WLTC cycle, due to a higher power demand from the cycle (see Fig. 5).

Fig. 5 shows the power demand obtained through TEST and VI-CarRealTime simulations; the battery network power, which is the battery pack power obtained in output from the "Datasheet Battery" subsystem; and the battery network power loss, that is an output variable of the "Datasheet Battery" subsystem.

As can be seen in Fig. 5, the power demand coincides with the battery network power, the power request from the vehicle system is therefore satisfied by the battery pack.

In Fig. 6 the following powers are compared: the opposite value of the battery network power loss (which is an output variable of the "Datasheet Battery" subsystem); and the heat generated by the batteries (calculated outside of "Datasheet Battery" subsystem, through the equation reported in section 3). Fig. 6 also shows the cooling heating power (calculated outside of "Datasheet Battery" subsystem, through the equation reported in section 3). Furthermore, the average cooling heating power on the WLTC cycle is shown by the dotted line.

Fig. 6 shows that the battery network power loss provided as output from the battery pack model changed in sign, equals the heat generated by the battery pack calculated through the equations reported in Section 3. From this, considering that the Simulink "Datasheet Battery" subsystem and the calculation laws reported in section 3 [43,44] are consolidated, it is possible to deduce that the internal resistance of the cells has been correctly estimated, considering the Panasonic 18650 LIB cell [50]. In fact, the "Datasheet Battery" subsystem calculates power losses, due to Joule effect, based on internal resistance.

From this first simulation, the average consumption on the WLTC cycle, class 3b, was calculated. First of all, for a battery SOC of 100 %, the open circuit voltage of the single cell is known, equal to 4.2 V. By multiplying this value by the number of cells placed in series ($N_s = 96$) it is possible to obtain the nominal open circuit voltage of the battery pack, equal to 403.2 V C_{bat} is defined as the battery pack energy and it is equal to $C_{cell} \bullet N_p$. Considering that C_{cell} is equal to 2.75 Ah and that the number of cells placed in parallel in the battery pack is equal to 59, the capacity of the battery pack is equal to 162.25 Ah. Multiplying C_{bat} by the open circuit voltage of the battery pack (with battery SOC equal to 100 %), it is possible to obtain an energy content of the battery pack (defined as C_{bat_kWh}) equal to 65.4192 kWh.

Considering the battery SOC at the beginning of the simulation (80 %) and the SOC obtained at the end of the simulation (67.5 %), a SOC variation (ΔSOC) of 12.5 % is required on the single WLTC cycle (class 3b).

Using the following equation, it is therefore possible to obtain the energy consumption on the WLTC, class 3b, cycle ($35.1317\, kWh/100\, km$): $C_{bat\_kWh} \bullet \Delta SOC / s_{WLTC}$, where s_{WLTC} is the distance travelled by the vehicle on the driving cycle considered, equal to 23.266 km.

The theoretical range of the vehicle achievable ideally discharging the battery pack from 100 % to 0 % SOC, will be calculated as the ratio between C_{bat_kWh} and the energy consumption on the considered driving cycle, and it is equal to 186.2 km for the case in exam. Finally, the range to discharge the battery pack from 100 % to 20 % SOC is instead calculated multiplying the previous range for 0.8, obtaining in this case a value of 149.0 km.

Therefore, the baseline vehicle is able to cover six WLTC cycles (class 3b) plus a small part of the seventh cycle before the SOC drops below 20 %, as can also be seen from Fig. 7.

Now, different sets of simulations are presented, for the baseline vehicle with active liquid-cooling system, composed of the repetition of WLTC cycles (class 3b), starting from SOC equal to 100 % until the SOC drops below 20 %. The simulation sets are repeated with different battery pack initial temperatures. The results of these sets of simulations are reported in Fig. 7. In this figure the

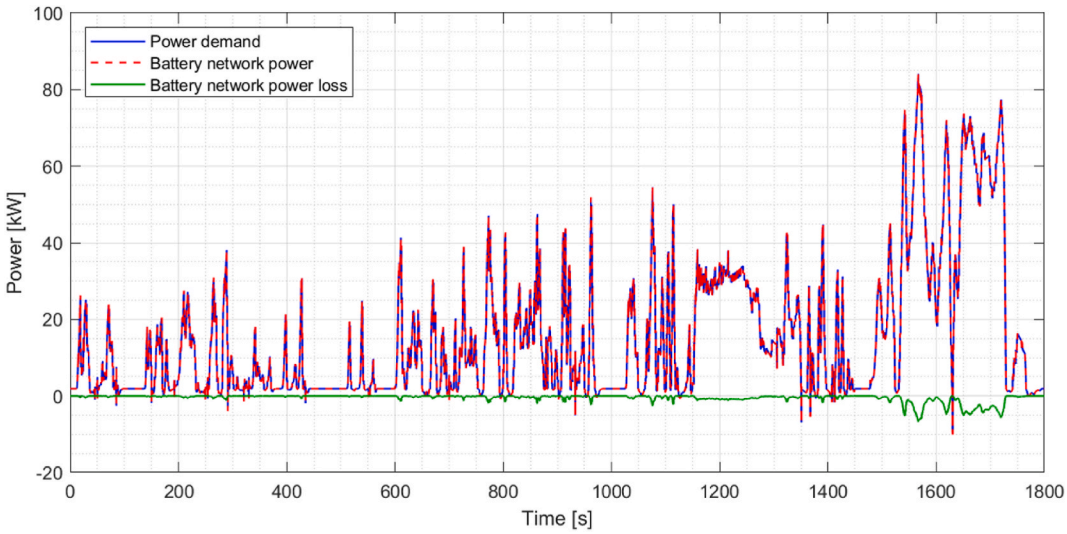

Fig. 5. Power. Power demand and battery network power loss.

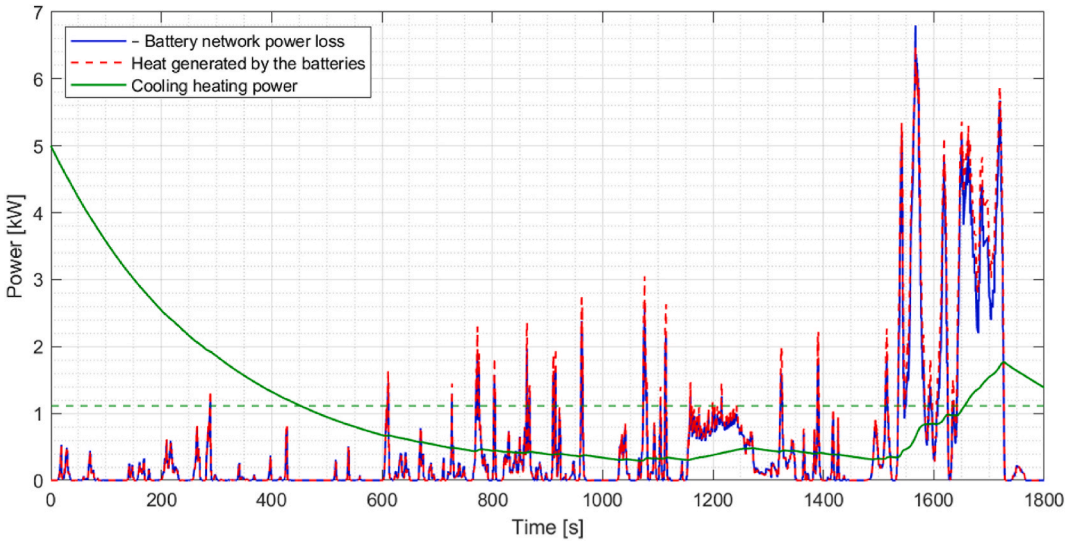

Fig. 6. Power comparison. Power lost from the battery pack in the form of heat and cooling heating power.

vertical red lines separate one WLTC cycle from the next, while the horizontal green line represents the minimum acceptable SOC (20 %).

Fig. 7a reports the battery SOC during the repetition of the WLTC driving cycles. Fig. 7b shows the tendency of the battery pack temperature to approach the temperature of the coolant during the first WLTC cycle. During the following cycles the temperature gradually tends to slowly rise in general, due to the high-power demand phase at the end of each cycle, but without ever deviating too much from 20 °C and hence remaining within the optimal operating range, until the battery pack is discharged (SOC below 20 %). Therefore, using the active liquid cooling system the operation of the vehicle is not limited by the temperature of the battery pack, but only by the maximum range that the battery pack can achieve, on the considered driving cycle.

From Fig. 7b, it can be observed that even starting from the limit temperature of 60 °C, the active liquid thermal conditioning system manages to bring the system back to around the optimal temperature of the battery pack, avoiding overheating.

Fig. 7c confirms what can be seen in the equation set described in section 3, the heat generated by the batteries increases as the residual capacity of the battery pack decreases. This is because the battery internal resistance grows as the SOC decreases. Fig. 7b and 7d shows that the cooling heating power and the average temperature of the battery pack have a similar trend over the simulation time.

Fig. 8 shows the cooling heating power on each WLTC (class 3b) cycle, and its average over the 7 simulated WLTC cycles (0.8185 kW), starting with 25 °C temperature for the battery pack, for the baseline vehicle with active liquid-cooling system. Even in this figure, the vertical red lines separate each WLTC cycle from the next.

It has been hypothesized to use the average value of the cooling heating power on the set of simulations with an initial battery temperature of 25 °C, as the average consumption of the battery thermal management system (see Fig. 8). This information will be needed for the vehicle configurations discussed in the next sections.

4.2. *Passive air-cooling vehicle*

In this case the same reference vehicle is considered, but without the active liquid-cooling thermal management system. It is therefore necessary to subtract the weight of the cooling system itself (88.84 kg) from the vehicle and reduce the auxiliary power consumption by 818.5 W. The additional weight given by the passive air-cooled system is considered zero, so it was assumed to have the same battery pack as the liquid-cooled system, but with enough space between the cells to allow the passage of air, which passes naturally during the movement of the vehicle. Therefore, no forced ventilation was assumed, so there is no system with a fan that adds additional weight. Subtracting the 815.5 W from the total power consumed by the vehicle's auxiliaries gives 681.5 W of average auxiliary power consumption. Moreover, by removing the 88.84 kg coming from the active liquid-cooling system, the total weight of the vehicle goes from 1986.6 kg to 1897.8 kg, i.e. a lightweighting of 4.5 % of the initial vehicle mass has been achieved.

Regarding the Simulink model of the battery pack, it was assumed that there is no heat exchange between the battery pack and the outside. All the heat generated by the battery pack therefore contributes to increase the temperature of the pack itself. This assumption is equivalent to $Q_{CP} = 0$. This assumption was made in such a way as to consider the worst-case scenario.

4.2.1. *Battery pack configuration: 96S59P*

Fig. 9 shows the results related to a simulation with the battery model with passive air cooling, starting from a battery SOC equal to 80 %, assuming an initial battery temperature equal to 25 °C. To obtain the power demand to be supplied as input to the battery model, the simulation with VI-CarRealTime software (with vehicle weight equal to 1897.8 kg) and the simulation with the TEST model

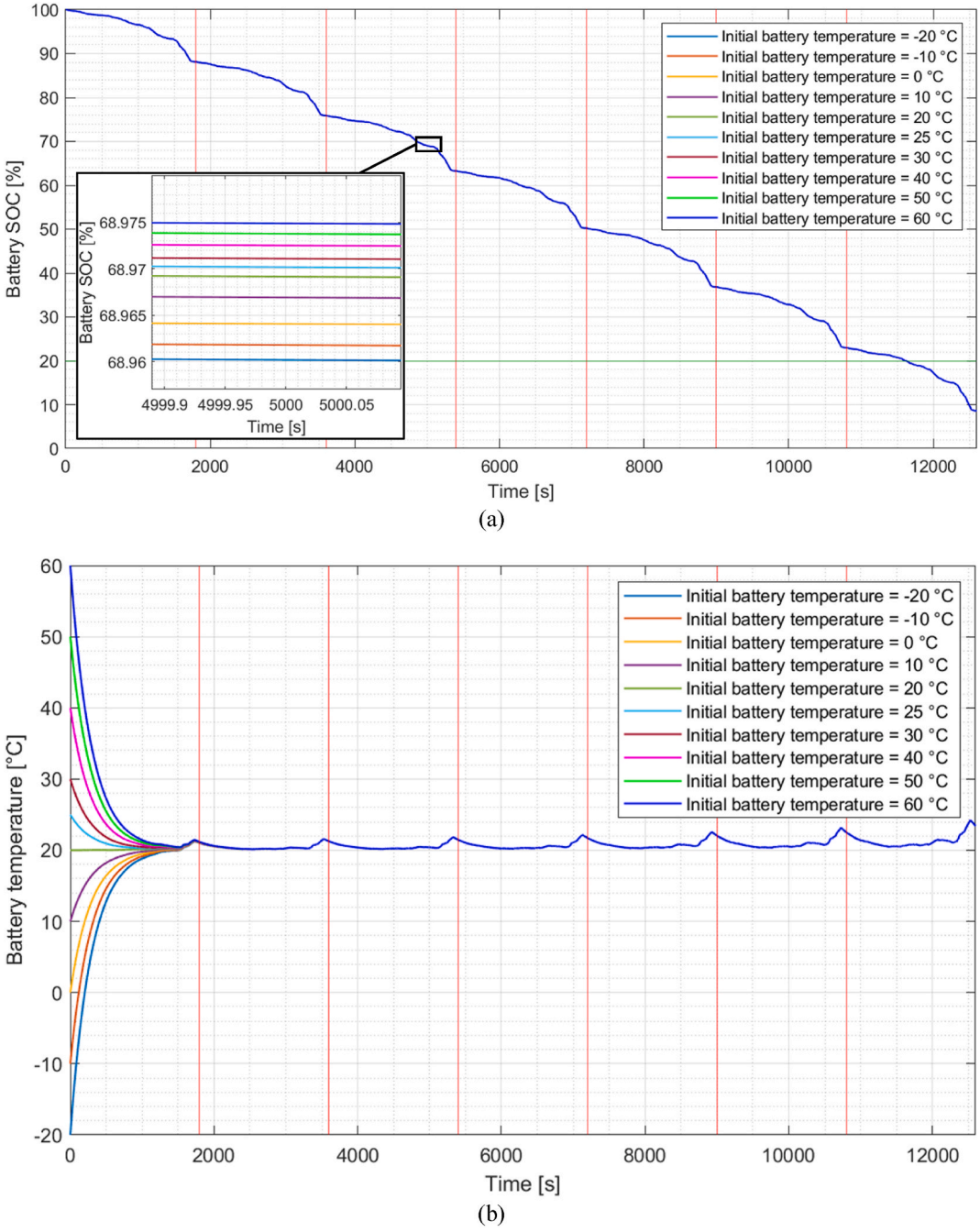

Fig. 7. WLTC repetitions for baseline vehicle with active liquid-cooling system. (a) battery SOC; (b) battery average temperature; (c) heat generated by the batteries; and (d) cooling heating power.

(considering an average power of all the vehicle's auxiliaries equal to 681.5 W) were repeated. In particular, Fig. 9a reports the battery current and the battery voltage during the entire simulation; Fig. 9b the battery SOC and the battery energy; and Fig. 9c shows the battery temperature.

In this case the average consumption on the WLTC cycle, class 3b, is 31.99 $kWh/_{100\,km}$, which is 91.06 % of the consumption achieved by the baseline vehicle with active liquid-cooling system. The final range of this lighter vehicle is 163.6 km, 9.82 % higher than the range of the baseline vehicle.

Now, for the passive air-cooled vehicle, different sets of simulations are presented, composed of the repetition of WLTC cycles (class

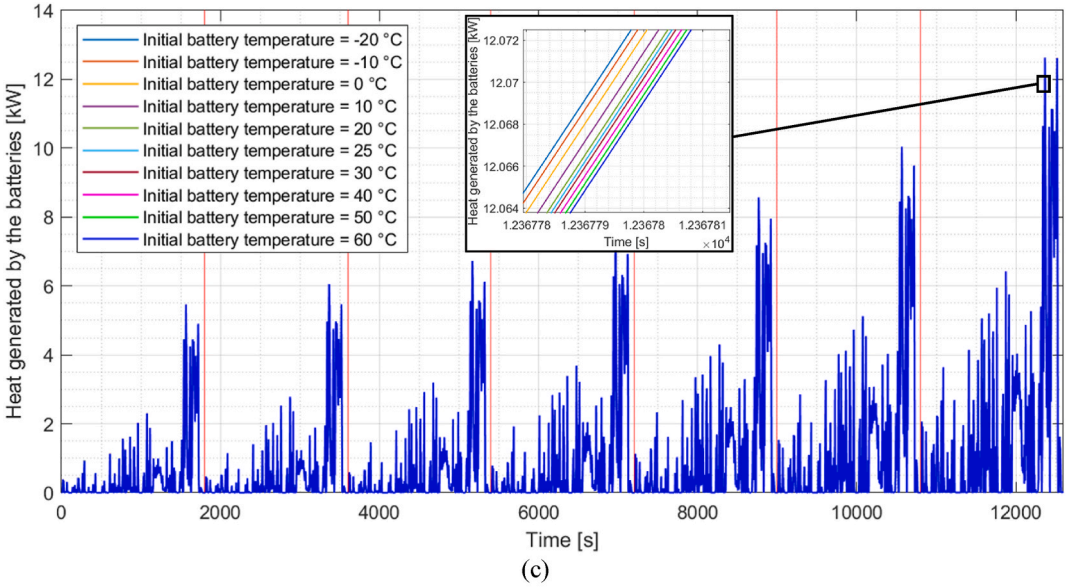

(c)

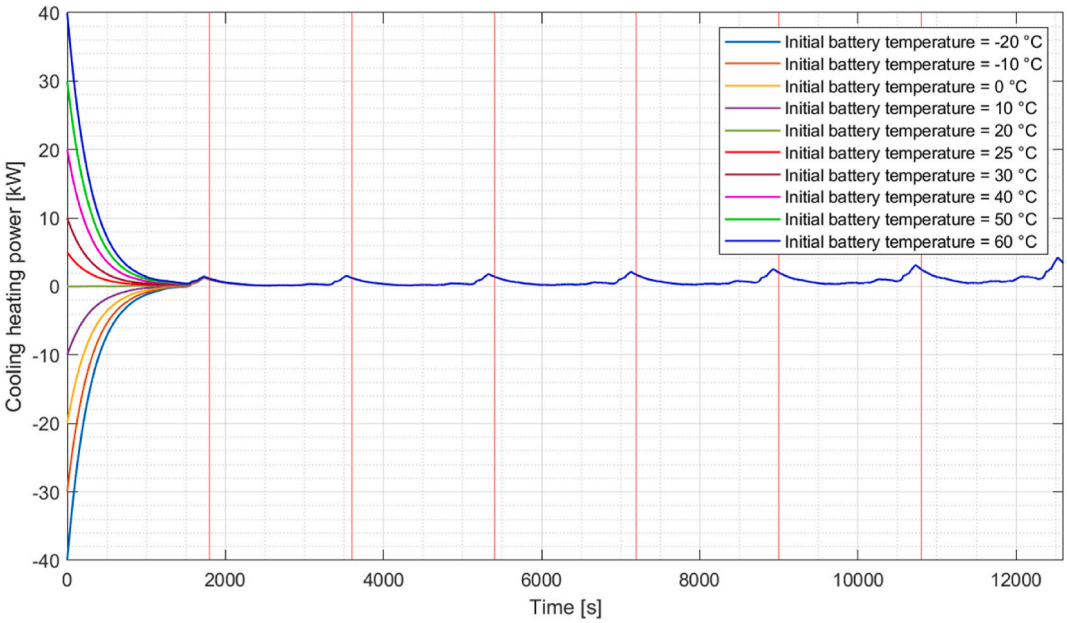

(d)

Fig. 7. (*continued*).

3b), starting from SOC equal to 100 % until the SOC drops below 20 % or until the battery temperature exceeds 60 °C. The limit temperature of 60 °C corresponds to the limit of the battery pack's discharge operating range. As for the baseline configuration, the simulation sets are repeated with different battery pack initial temperatures. The results of these sets of simulations are reported in Fig. 10. Even in this figure, the vertical red lines separate one WLTC cycle from the next, while the horizontal green line represents the 20 % of SOC, and the dotted horizontal red line represents the maximum temperature limit, equal to 60 °C.

Compared to the previous configuration (active cooled battery pack in configuration 96S59P), the difference in SOC between the various simulations is more visible, especially below approximately 50 % of SOC as can be seen in Fig. 10a. This is due to the different initial temperature of the battery pack between each set of simulations, as can be seen from Fig. 10b.

As shown in Fig. 10b, for initial temperatures ranging from −20 °C to 30 °C, the vehicle's limitation is the battery pack's capacity, reaching a SOC of 20 %. However, for simulations starting at 40 °C and above, the limiting factor becomes the pack's temperature, reaching the 60 °C threshold. Consequently, at these higher temperatures, the vehicle can only travel a limited distance before needing

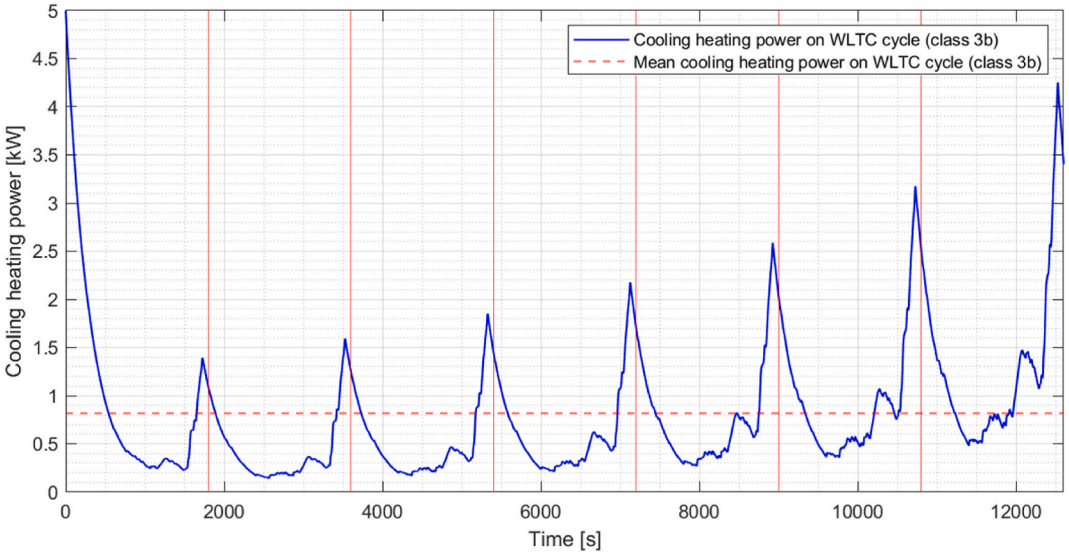

Fig. 8. Cooling heating power. Baseline vehicle with active liquid-cooling system. This graph refers to the set of simulations with an initial battery temperature of 25 °C.

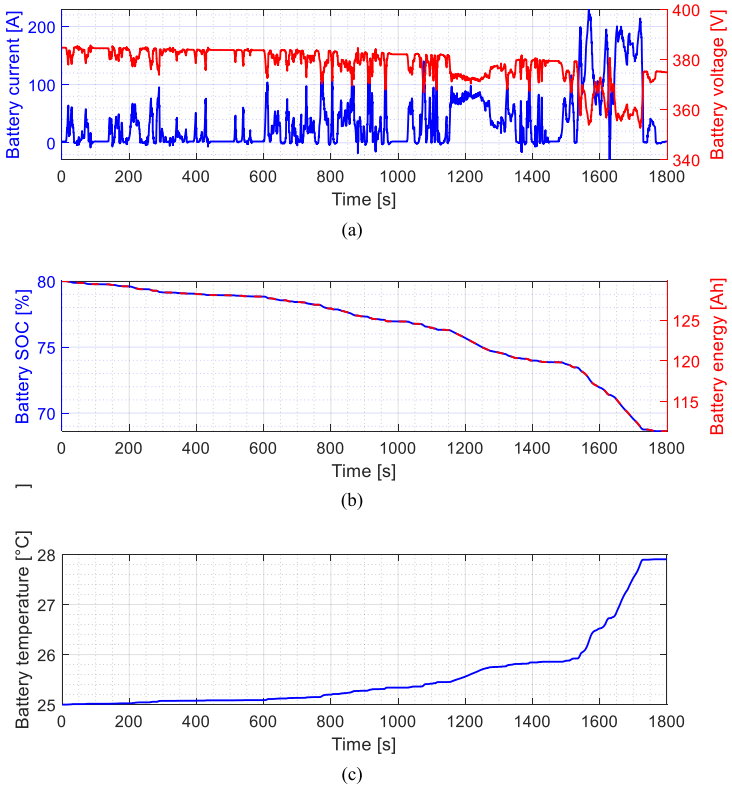

Fig. 9. Results for the vehicle with air-cooled battery pack (96S59P). Results in terms of (a) battery current and battery voltage; (b) battery SOC and battery energy; (c) battery temperature.

to stop for the battery pack to cool down. This means it is impossible to fully utilize the battery pack's range continuously (as per the WLTC cycle, class 3b).

This air-cooled system is best suited for environments where the battery pack does not exceed approximately 30 °C before the vehicle starts. However, it is important to note that a high initial battery pack temperature may result not only from high ambient

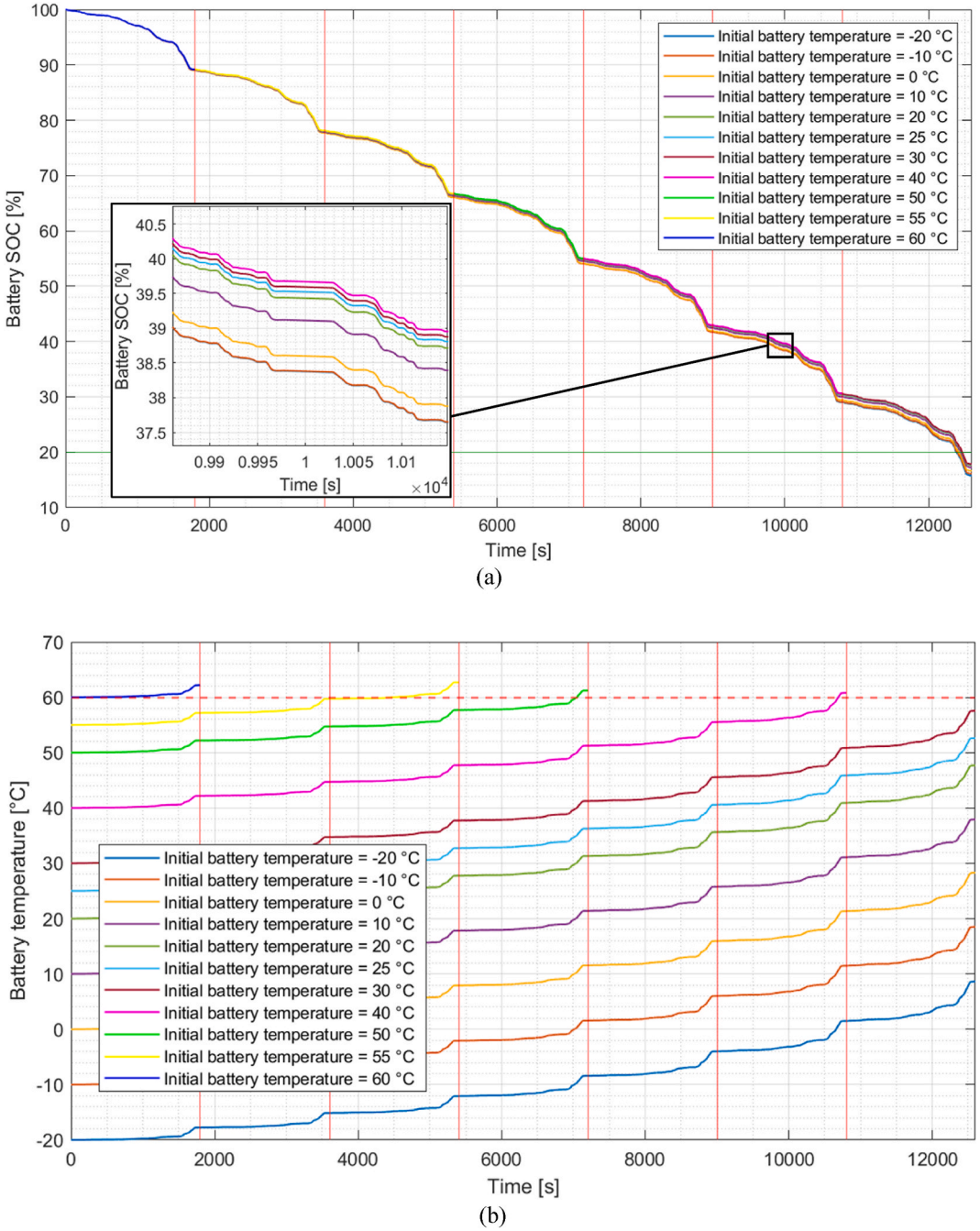

Fig. 10. WLTC repetitions for the vehicle with passive air-cooled battery pack (96S59P). (a) battery SOC; and (b) battery average temperature.

temperatures but also from previous vehicle use. For extreme temperature conditions, this battery model could be adapted for fleet vehicles with predefined missions, where operating conditions are controlled and planned.

The simulation set starting with a battery pack temperature of 60 °C includes only one simulation, beginning with an initial SOC of 100 %. Due to the assumptions in the air-cooled battery pack model, the pack temperature can only rise during simulations, and 60 °C is the maximum allowable temperature. Therefore, starting from 60 °C, the battery pack immediately overheats, as this passive air system is not able to re-establish the optimal temperature of the pack. The same thing will be seen below also for the air-cooled battery pack in configuration 96S54P.

4.2.2. Battery pack configuration: 96S54P (secondary lightweighting)

Given that the vehicle with an air-cooled battery pack consumes 91.06 % of the energy used by the same vehicle with an active-cooled battery pack, we decided to reduce the number of cells in the air-cooled battery pack to achieve the same range of the baseline vehicle. This ensures the air-cooled battery pack has a capacity of approximately 91.06 % of the reference battery pack (configured as 96S59P), equating to roughly 147.74 Ah compared to the original 162.25 Ah.

To achieve this, about 53.7 cells are needed in parallel (since each cell has a capacity of 2.75 Ah). We rounded this to 54 cells in parallel, resulting in a configuration of 96S54P. With 96 cells in series, reducing the parallel cells from 59 to 54 reduces the total number of cells by 480 (5 cells x 96).

Considering each cell's density ($\rho_{bat} = 2841.5\ kg/m^3$) and volume ($v_{bat} = 1.654 \bullet 10^{-5}\ m^3$), the weight of a single cell is 0.047 kg. Thus, reducing the battery pack by 480 cells results in a mass reduction of 22.559 kg (0.047 kg x 480). Although there would be additional weight savings from fewer wires and a potentially lighter cell container, we consider this negligible compared to the 22.6 kg reduction from fewer cells.

Therefore, we repeated the simulations, reducing the vehicle's total weight by another 22.559 kg. This is in addition to the 88.84 kg reduction from the absence of the active-cooling system (primary lightweight), totalling a weight reduction of 111.399 kg. The new vehicle configuration, with an average auxiliary power of 681.5 W, has a total weight of about 1875.2 kg, achieving a further 5.6 % mass reduction from the reference vehicle's weight of 1986.6 kg.

Fig. 11 presents the simulation results for the 96S54P battery model with passive air cooling, starting from a battery SOC of 80 % and an initial battery temperature of 25 °C. In particular, Fig. 11a reports the battery current and the battery voltage during the entire simulation; Fig. 11b the battery SOC and the battery energy; and Fig. 11c shows the battery temperature.

After the secondary lightweight, the average consumption on the WLTC cycle, class 3b, is 31.96 kWh per 100 km, which is 90.96 % of the consumption of the baseline active-cooled vehicle. The range to deplete 80 % of the SOC of the battery pack is 149.9 km, only 0.62 % higher than that of the active-cooled vehicle. Thus, the air-cooled vehicle with 480 fewer cells achieves a range comparable to the baseline car.

For this vehicle configuration, further sets of simulations are presented. These simulations consist of repeating WLTC cycles (class 3b), starting from a SOC of 100 % and continuing until the SOC drops below 20 % or the battery temperature exceeds 60 °C. The results of these simulations are shown in Fig. 12. Even in this figure, the vertical red lines separate one WLTC cycle from the next, while the horizontal green line represents the 20 % of SOC, and the dotted horizontal red line represents the maximum temperature limit, equal to 60 °C.

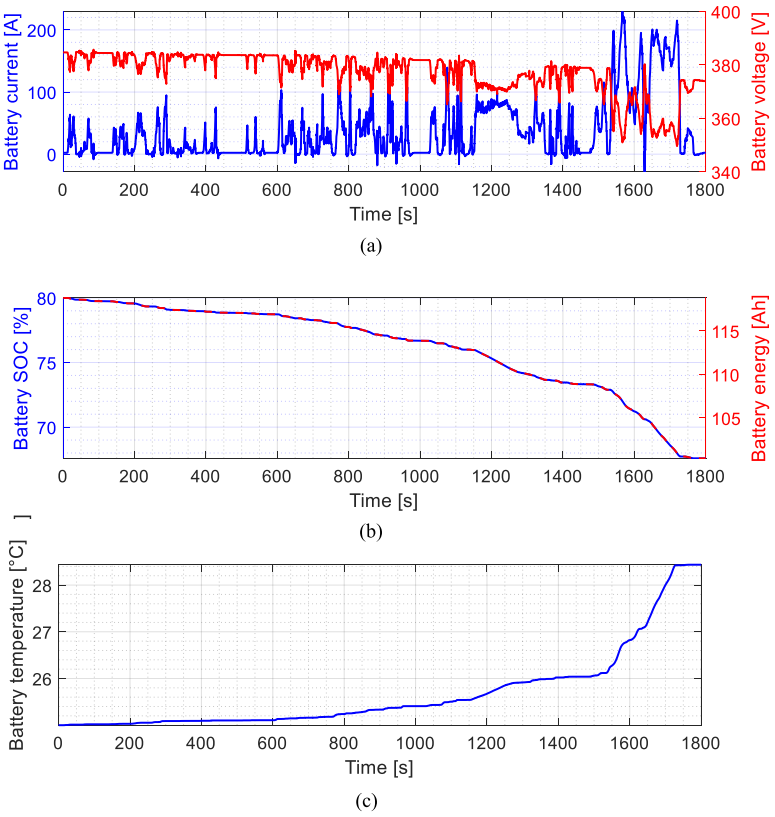

Fig. 11. Results for the vehicle with air-cooled battery pack (96S54P). Results in terms of (a) battery current and battery voltage; (b) battery SOC and battery energy; (c) battery temperature.

Again, compared to the case with active cooling, the difference in SOC between the various simulations is more perceptible especially below approximately 50 % of SOC, as it can be seen in Fig. 12a.

As before, the set of simulations starting with a battery pack temperature of 60 °C includes only one simulation, with an initial SOC of 100 %.

Fig. 12b shows that for initial temperatures from −20 °C to 30 °C, the vehicle is limited by the battery pack's capacity. For simulations starting at 40 °C and above, the limiting factor is the battery pack reaching the 60 °C threshold. Consequently, this system is well-suited for fleet vehicles with programmable and predefined missions.

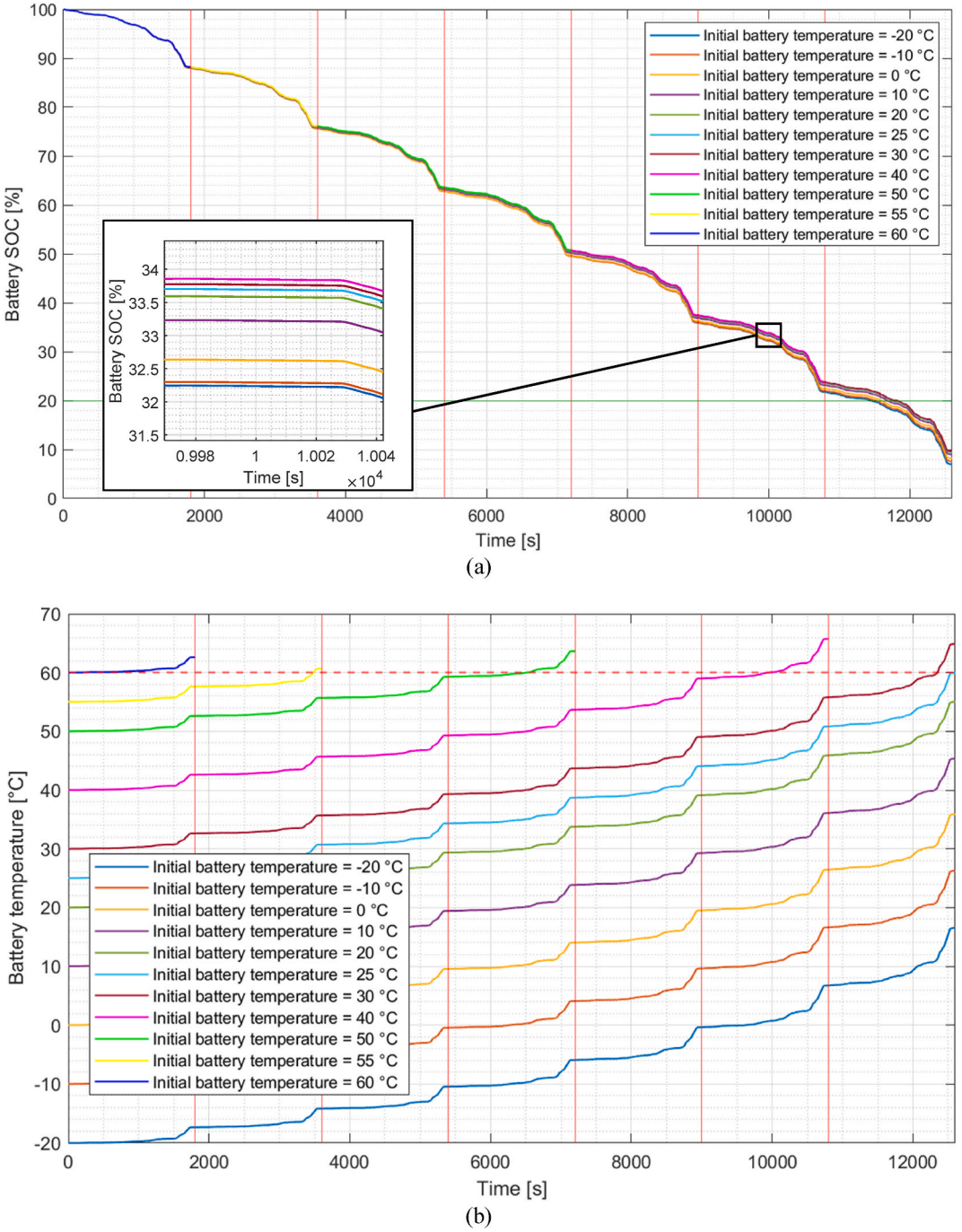

Fig. 12. WLTC repetitions for the vehicle with passive air-cooled battery pack (96S54P). (a) battery SOC; and (b) battery average temperature.

4.3. Passive PCM (phase change material) cooling system

In the case of the passive PCM (Phase Change Material) cooling system, the same reference vehicle is considered, but once again without the active liquid-cooling thermal management system. Therefore, the weight (88.84 kg) and the auxiliary power consumption (818.5 W) of the active cooling system are subtracted from the vehicle. Additionally, it is necessary to add the weight of the PCM material considered, which in these systems forms a containment structure for the cells, in which the cells themselves are completely immersed. It is also assumed that the volume occupied by the cell and the PCM is equal to a parallelepiped with sides 70 mm•70 mm•19 mm (25.27 cm^3), considering that the single cell has a diameter of approximately 18.4 mm and a length of approximately 65 mm. Subtracting the volume of the cell (v_{cell}) from the volume of 25.27 cm^3 gives the volume of PCM associated with the single cell, equal to 8.73 cm^3.

In the Simulink model of the battery pack, it is assumed that there is no heat exchange between the battery pack and the environment. All the heat generated by the battery pack increases the pack's temperature ($Q_{CP} = 0$) until it reaches the melting point of the chosen PCM. Once the melting point is reached, the battery pack's temperature remains constant until the heat generated (sum of Q_{bat}/dt, from the melting point onwards) reaches the limit of the PCM's heat absorption capacity (maximum energy absorbed by the PCM during the phase change, Q_{PCM}). After this limit is reached, the temperature begins to rise again according to the previously explained calculation method (section 3), with Q_{CP} remaining zero. These assumptions are made to represent the worst-case scenario in a simplified manner.

The maximum energy absorbed by the PCM during the phase change (Q_{PCM}) is defined as in equation (4).

$$Q_{PCM} = m_{PCM} \bullet N_p \bullet N_s \bullet L_{PCM} \tag{4}$$

where m_{PCM} is the mass of the PCM associated with the single cell of the battery pack and L_{PCM} is the latent heat of the selected PCM.

4.3.1. PCM: glycerol

Glycerol ($C_3H_8O_3$), an organic phase change materials [52], was chosen as the PCM for the case studied in this section. Multiplying the volume of PCM associated with the single cell by the density of the glycerol gives the mass of this PCM associated with the single cell, equal to 0.011 kg.

4.3.1.1. Battery pack configuration: 96S59P. If the reference 96S59P battery pack configuration is considered, the total mass of the PCM corresponds to 62.303 kg (mass associated with the single cell for the number of total cells, i.e. 96•59 = 5664). Table 4 resume the main characteristics of the glycerol PCM used for this configuration, and the main PCM data of the others configuration exposed in the next subsections.

The simulations have been repeated subtracting the weight of the cooling system (88.84 kg) from the reference vehicle, and adding the total mass given by the PCM (62.303 kg), achieving a total of 26.537 kg of lightweighting (new total vehicle weight equal to 1960.1 kg). The average power consumed by the auxiliaries was once again set to 681.5 W, to obtain the new power demand from TEST model.

Fig. 13 shows the results of a single battery pack simulation, for the WLTC driving cycle, class 3b, starting from a SOC of 80 % and from an initial battery pack temperature of 25 °C. In particular, Fig. 13a reports the battery current and the battery voltage during the entire simulation; Fig. 13b the battery SOC and the battery energy; Fig. 13c shows the battery temperature; and Fig. 13d the energy absorbed by the glycerol PCM during the phase change.

In the glycerol PCM cooling system configuration, the average consumption on the WLTC cycle, class 3b, is 32.45 kWh per 100 km, which is 92.38 % of the consumption of the active-cooled vehicle and only 1.45 % more than the same air-cooled vehicle model (96S59P). The range to deplete 80 % of the SOC of the battery pack is 161.3 km, 8.25 % higher than the range of the active liquid-cooled vehicle and only 1.42 % less than the same air-cooled vehicle (96S59P).

As for the previous configurations, various sets of simulations have been carried out, consisting of repeating WLTC cycles (class 3b) starting from a SOC of 100 % and continuing until the SOC drops below 20 % or the battery temperature exceeds 60 °C.

An assumption was made for the set of simulations starting from an initial battery pack temperature of 26 °C: it is assumed that the battery pack has just reached this temperature at the start of the first simulation, so the initial value of Q_{PCM} is zero. For subsequent simulations starting from 30 °C and above, the phase transition of the PCM is considered complete. The system, based on these assumptions, behaves similarly to the air-cooled case but with a slightly higher vehicle weight and power demand.

The results of these simulations are presented in Fig. 14. Even in this figure, the vertical red lines separate one WLTC cycle from the next, while the horizontal green line in Fig. 14a represents the 20 % of SOC, and the dotted horizontal red line in Fig. 14b represents the maximum temperature limit, equal to 60 °C.

Once again, the difference in SOC between the various simulations becomes more noticeable, particularly below approximately 50 % SOC, as shown in Fig. 14a. This difference is linked to temperature, as illustrated in Fig. 14b. Fig. 14c instead shows the energy absorbed by PCM during the repetition of the WLTC cycles.

For simulation sets with an initial battery pack temperature below 0 °C, the temperature never reaches the 26 °C melting point of the PCM, resulting in behaviour similar to the air-cooled case. For initial temperatures between 0 °C and 25 °C, the battery pack reaches 26 °C during the simulations and maintains this temperature until the SOC drops to 20 %. For initial temperatures above 26 °C, the temperature trend mirrors that of the air-cooled case, with the vehicle being limited by reaching the 60 °C threshold.

Here too, starting from 60 °C the battery pack immediately experiences overheating. In fact, since the melting point temperature of

Table 4
Main characteristics of the PCMs chosen for the studies.

PCM	Melting point[°C]	Latent heat [J/kg]	PCM Density [kg/m^3]	Volume (PCM + cell)[m^3]	Cell volume [m^3]	PCM volume [m^3]	PCM mass [kg]	N_s	N_p	PCM mass (in the pack)[kg]
Glycerol	26[a]	184 000[a]	1260	$2.527 \bullet 10^{-7}$	$1.654 \bullet 10^{-7}$	$8.73 \bullet 10^{-6}$	0.011	96	59	62.303
	26[a]	184 000[a]	1260	$2.527 \bullet 10^{-7}$	$1.654 \bullet 10^{-7}$	$8.73 \bullet 10^{-6}$	0.011	96	54	57.023
Stearyl alcohol	57[a]	242 850[a]	812.4[b]	$2.527 \bullet 10^{-7}$	$1.654 \bullet 10^{-7}$	$8.73 \bullet 10^{-6}$	0.007	96	59	40.171
	57[a]	242 850[a]	812.4[b]	$2.527 \bullet 10^{-7}$	$1.654 \bullet 10^{-7}$	$8.73 \bullet 10^{-6}$	0.007	96	54	36.766

[a] Ref. [52].
[b] Ref. [53].

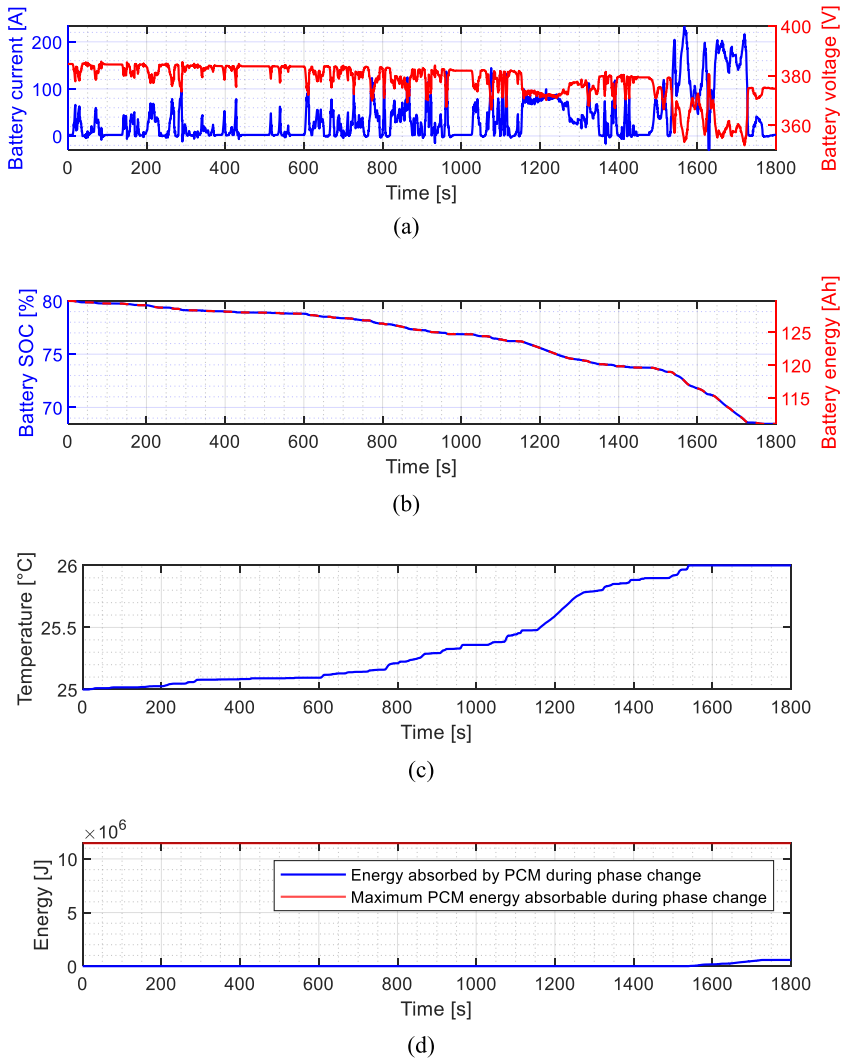

Fig. 13. Results for the vehicle with passive glycerol PCM cooled battery pack (96S59P). Results in terms of (a) battery current and battery voltage; (b) battery SOC and battery energy; (c) battery temperature; (d) energy absorbed by the glycerol PCM during the phase change.

the glycerol PCM is 26 °C, and therefore lower than 60 °C, the behaviour of the system is similar to that of the air-cooled system. The same will also be shown for the glycerol PCM-cooled battery pack in 96S54P configuration and for the battery pack with stearyl alcohol PCM cooling system (for both battery pack configurations). In fact, even stearyl alcohol has a melting point temperature lower than 60 °C, in particular equal to 57 °C.

This glycerol PCM-cooled system is particularly suited to environments where the battery pack does not exceed approximately 30 °C before vehicle operation, making it ideal for fleet vehicles with controlled and programmed missions. The advantage of this solution is that it allows the battery pack to operate at an optimal temperature for initial temperatures below 26 °C, which helps reduce cell degradation over time.

4.3.1.2. Battery pack configuration: 96S54P (secondary lightweighting). Given that the vehicle with the glycerol PCM cooling system consumes 92.38 % of the energy used by the baseline active liquid-cooled vehicle, we decided to reduce the number of cells in the battery pack to match this efficiency and therefore achieving a secondary lightweighting. This reduction brings the battery pack's capacity to approximately 149.89 Ah, compared to the reference 162.25 Ah. To achieve this, around 54.5 cells are needed in parallel (since each cell has a capacity of 2.75 Ah). We chose to use 54 cells in parallel, rounding down. By reducing the number of cells and the vehicle's weight, consumption is further reduced, requiring slightly less battery capacity to complete the same driving cycle. In the new 96S54P configuration, the reduction of 480 cells results in a weight decrease of 22.559 kg.

All simulations were then repeated, incorporating this weight reduction of 22.559 kg. In the 96S54P battery pack configuration, the total mass of the PCM is 57.023 kg, based on the single cell's PCM mass for the total number of cells (96 x 54 = 5184).

The VI-CarRealTime simulation was repeated with the reference vehicle's mass, subtracting the active cooling system weight

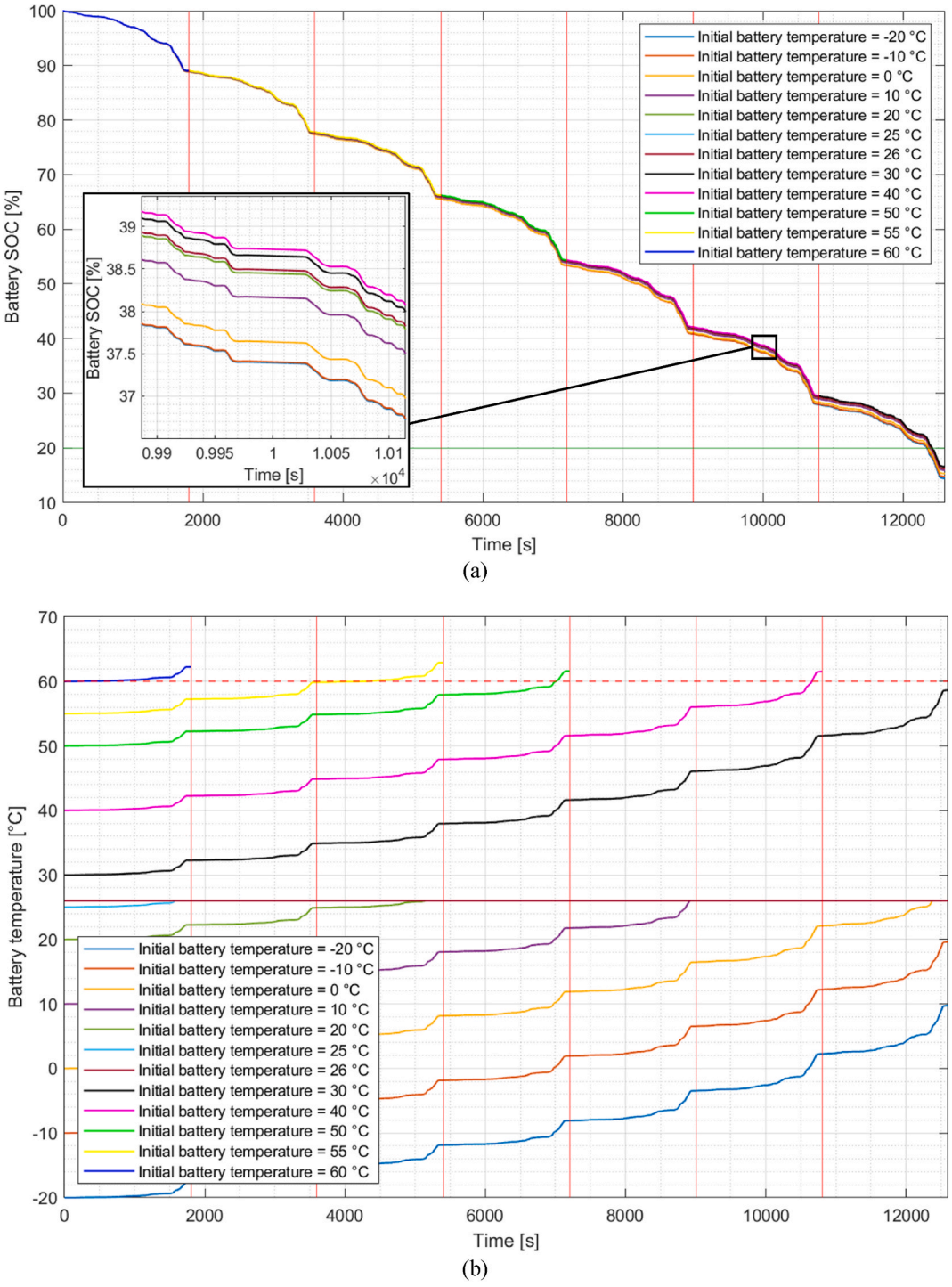

Fig. 14. WLTC repetitions for the vehicle with passive glycerol PCM cooled battery pack (96S59P). (a) battery SOC; (b) battery average temperature; and (c) energy absorbed by PCM during phase change.

(88.84 kg), adding the total PCM mass (57.023 kg), and subtracting the weight of the 480 removed cells (22.6 kg). This results in a total weight reduction of 54.417 kg, bringing the final vehicle weight to approximately 1932.2 kg. The TEST model simulation was also repeated with the new motor torques and angular speeds, considering the average power consumed by the auxiliaries to be 681.5 W. With the adjusted power demand, new results were obtained using the Simulink model of the battery pack.

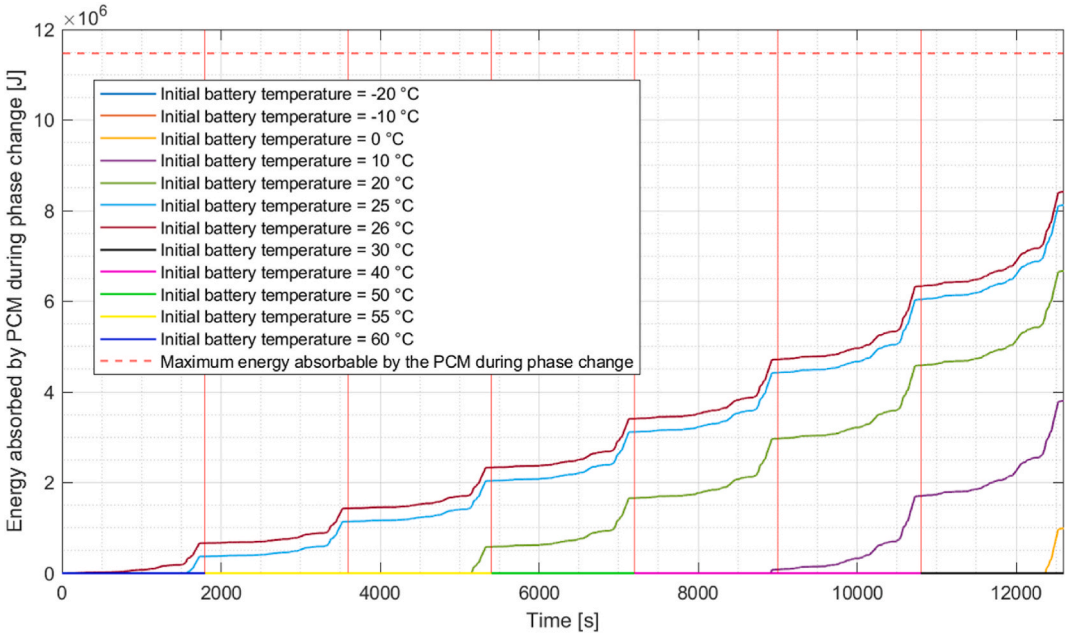

Fig. 14. (*continued*).

Fig. 15 shows the battery performance in the above-mentioned configuration on the WLTC driving cycle, class 3b, starting from a SOC of 80 % and an initial battery pack temperature of 25 °C. In particular, Fig. 15a reports the battery current and the battery voltage during the entire simulation; Fig. 15b the battery SOC and the battery energy; Fig. 15c shows the battery temperature; and Fig. 15d the energy absorbed by the glycerol PCM during the phase change.

In this glycerol PCM cooling scenario, the average energy consumption on the WLTC cycle, class 3b, stands at 32.39 kWh per 100 km, which is 92.18 % of the consumption of the actively liquid-cooled vehicle and only 1.34 % higher than the corresponding air-cooled model (96S54P). Similarly, the range to discharge 80 % of the battery pack's SOC equates to 147.9 km, 0.71 % less than the actively cooled vehicle and just 1.33 % lower than the air-cooled model (96S54P).

Furthermore, for this passive PCM-cooled vehicle, various sets of simulations are presented, again consisting of repetitions of WLTC cycles (class 3b). These simulations start from a SOC of 100 % and continue until the SOC drops below 20 % or until the battery temperature exceeds 60 °C. The results of these simulations are shown in Fig. 16. Once again, the same assumptions regarding Q_{PCM} are applied to simulations starting from an initial battery temperature of 26 °C or higher, consistently to those made in the previous case. Even in Fig. 16, the vertical red lines separate one WLTC cycle from the next, while the horizontal green line in Fig. 16a represents the 20 % of SOC, and the dotted horizontal red line in Fig. 16b represents the maximum temperature limit, equal to 60 °C.

Again, the difference in SOC between the different sets of simulations is more perceptible below approximately 50 % of SOC, as can be observed from Fig. 16a. The reason is once again associated with temperature (see Fig. 16b).

As shown in Fig. 16b, temperatures exceeding 26 °C exhibit a trend akin to the air-cooled scenario, where the limiting factor for the vehicle remains the 60 °C temperature threshold. In simulations starting with a battery pack temperature of 26 °C, this temperature persists until the conclusion of the final simulation. Conversely, for initial battery pack temperatures below 26 °C, once this temperature is reached, it remains constant throughout the simulation. Notably, only in cases where the initial battery pack temperature is 20 °C, the melting point temperature of the PCM is not attained (also referenced in Fig. 16c).

Once more, the glycerol PCM-cooled vehicle proves highly suitable for environments where the battery pack temperature remains below approximately 30 °C prior to vehicle operation. This makes it particularly well-suited for fleet vehicles. By utilizing this solution, the battery pack can operate at an optimal temperature, especially for initial temperatures below 26 °C, thereby mitigating cell degradation over time.

4.3.2. PCM: stearyl alcohol

Stearyl alcohol ($C_{18}H_{38}O$, 1-octadecyl alcohol), an organic phase change materials [52], has been chosen as the PCM for a further configuration studied in this section. Multiplying the volume of PCM associated with the single cell by the density of the glycerol gives the mass of this PCM associated with the single cell, equal to 0.007 kg.

4.3.2.1. Battery pack configuration: 96S59P. If the reference 96S59P battery pack configuration is considered, the total mass of the PCM corresponds to 40.171 kg. Table 4 resume also the main characteristics of the stearyl alcohol PCM in the 96S59P battery pack.

Both VI-CarRealTime and TEST model simulations have been repeated, subtracting the weight of the cooling system (88.84 kg)

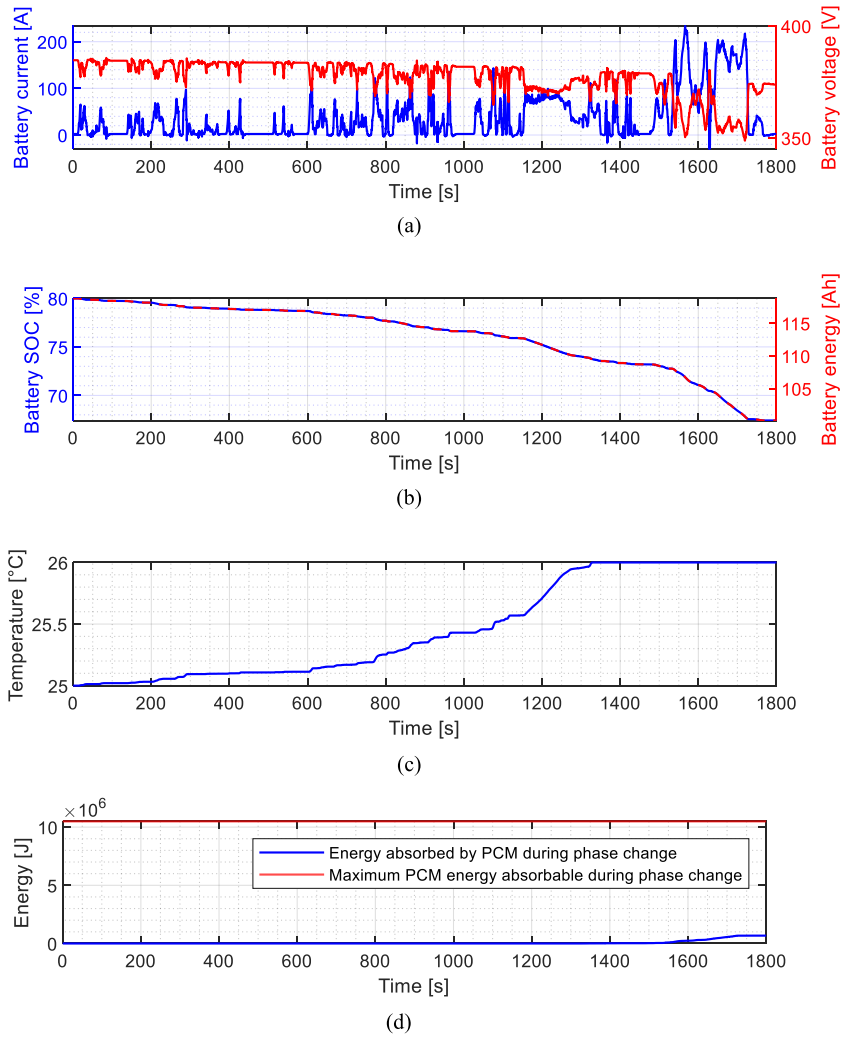

Fig. 15. Results for the vehicle with passive glycerol PCM cooled battery pack (96S54P). Results in terms of (a) battery current and battery voltage; (b) battery SOC and battery energy; (c) battery temperature; (d) energy absorbed by the glycerol PCM during the phase change.

from the reference vehicle, and adding the total mass given by the PCM (40.171 kg), for a total of 48.669 kg of lightweighting (new total vehicle weight equal to 1937.9 kg). Once again, auxiliary power has been set equal to 681.5 W. This power demand was used as input to the battery model to obtain the results shown below.

Fig. 17 shows the results of a single battery pack simulation for the WLTC driving cycle, class 3b, starting from a SOC of 80 % and from an initial battery pack temperature of 25 °C. In particular, Fig. 17a reports the battery current and the battery voltage during the entire simulation; Fig. 17b the battery SOC and the battery energy; Fig. 17c shows the battery temperature; and Fig. 17d the energy absorbed by the stearyl alcohol PCM during the phase change.

Using the stearyl alcohol PCM cooling configuration, the average energy consumption on the WLTC cycle, class 3b, stands at 32.28 kWh per 100 km, representing 91.90 % of the consumption of the actively liquid-cooled vehicle and only 0.92 % higher than the air-cooled vehicle (96S59P). Similarly, the range to discharge 80 % of the battery pack's SOC reaches 162.1 km, marking an 8.82 % increase over the actively liquid-cooled vehicle and 0.91 % less than the corresponding air-cooled vehicle (96S59P).

Now, for this passive PCM-cooled vehicle, various sets of simulations are presented, once again comprising repetitions of WLTC cycles (class 3b). These simulations start from a SOC of 100 % and continue until the SOC drops below 20 % or until the battery temperature raises over 60 °C.

An assumption is made for the set of simulations starting from an initial battery pack temperature of 57 °C: it is presumed that the battery pack has just reached this temperature at the onset of the first simulation, with the initial Q_{PCM} value set to zero. Conversely, for the final set of simulations, beginning from 60 °C regarding the initial battery pack temperature, the PCM's phase transition is deemed to have already been completed.

The outcomes of these simulation sets are shown in Fig. 18. Even in this figure, the vertical red lines separate one WLTC cycle from the next, while the horizontal green line in Fig. 18a represents the 20 % of SOC, and the dotted horizontal red line in Fig. 18b represents

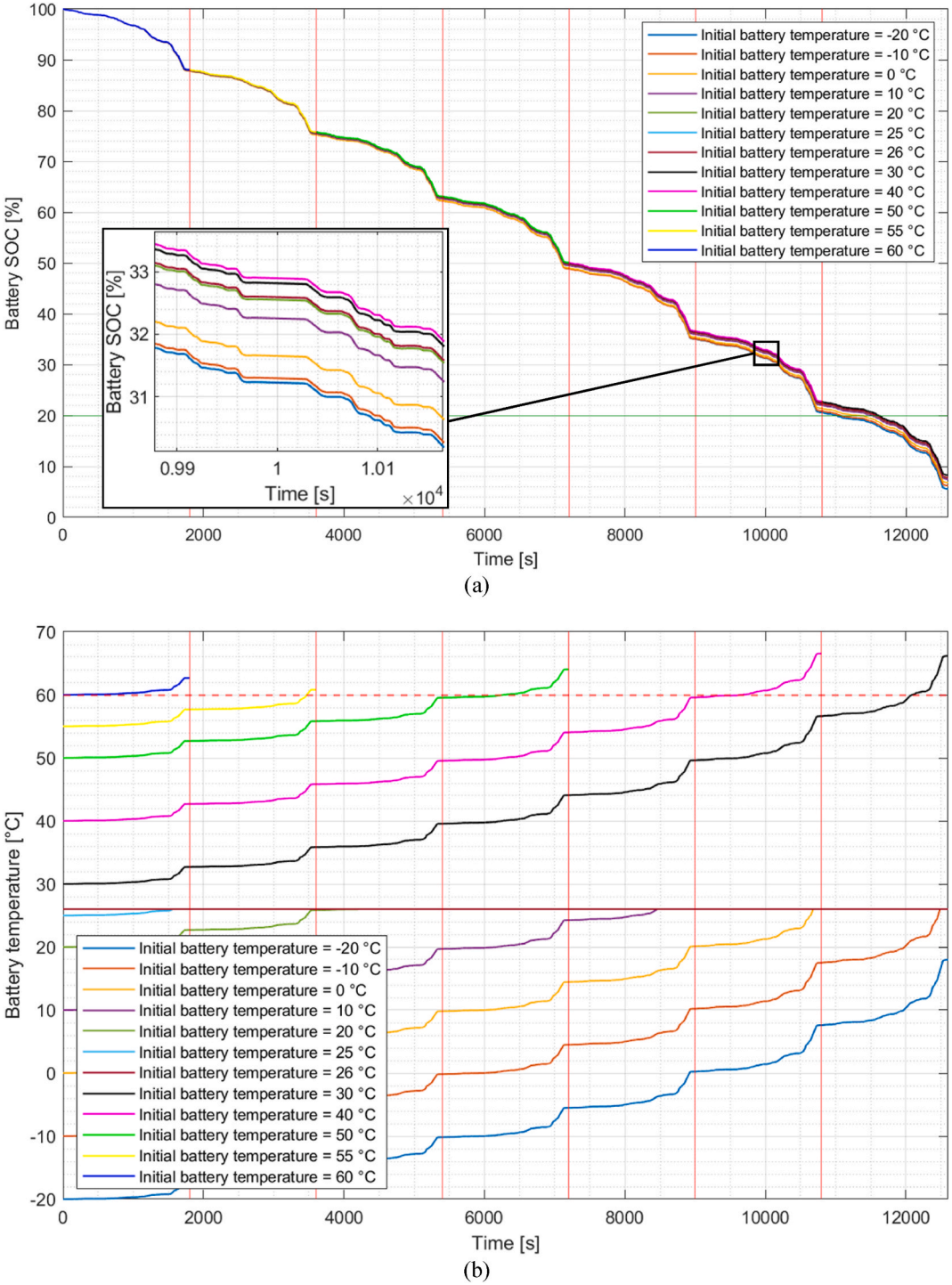

Fig. 16. WLTC repetitions for the vehicle with passive glycerol PCM cooled battery pack (59S54P). (a) battery SOC; (b) battery average temperature; and (c) energy absorbed by PCM during phase change.

the maximum temperature limit, equal to 60 °C.

The trend and conclusions on the battery state of charge are the same as for the air-cooled and glycol PCM-cooled configurations (see Fig. 18a, 18.b, and 18.c).

As shown in Fig. 18b, the simulation sets featuring initial battery pack temperatures up to 25 °C never reach the temperature of

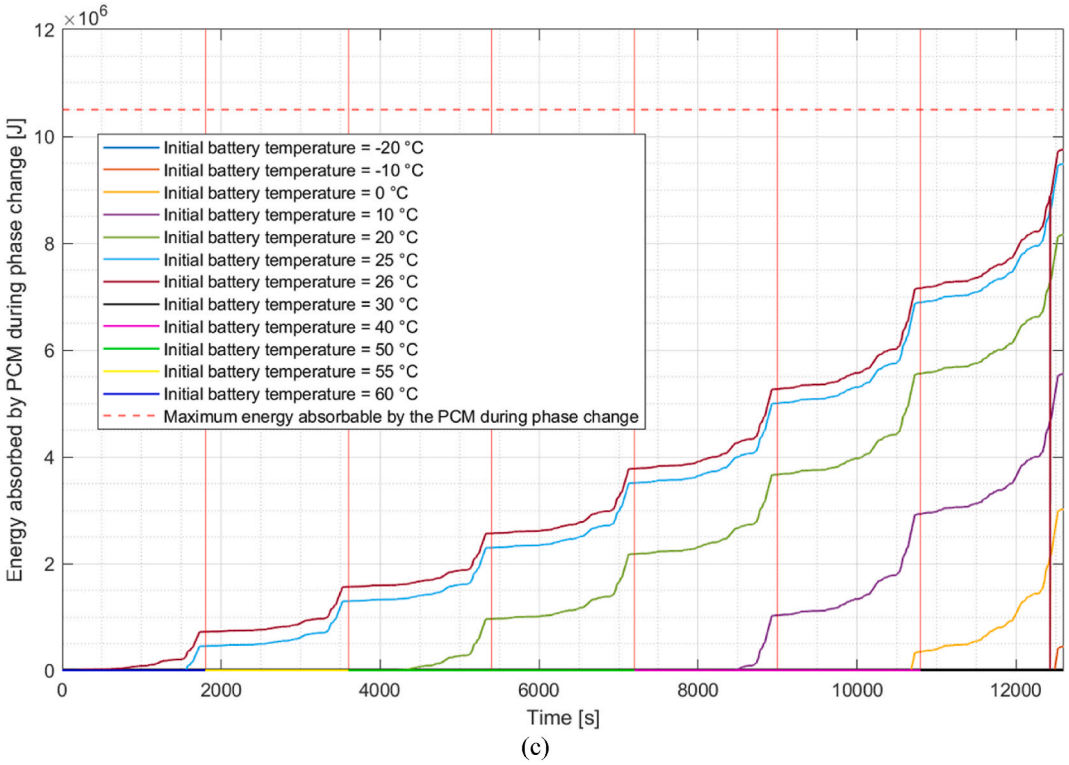

Fig. 16. (*continued*).

57 °C, which corresponds to the melting point of the PCM under consideration. Conversely, for sets beginning from 30 to 55 °C, the battery pack attains the temperature of 57 °C and sustains it until the conclusion of the final simulation. Even when commencing from 57 °C, the battery pack maintains this temperature until the end of the last simulation. Notably, the scenario starting from an initial battery pack temperature of 60 °C mirrors that of air-cooled batteries, with the temperature steadily increasing throughout.

The vehicle equipped with this PCM cooling system, featuring a melting point of 57 °C, is suitable for daily use as well as for fleet operations, provided the initial battery pack temperature does not exceed 57 °C. The key advantage of this solution is its ability to keep the battery pack temperature below 60 °C, even starting from high initial temperatures. However, compared to the previous system with a PCM melting point of 26 °C, this configuration does not maintain the battery pack within an optimal temperature range, potentially leading to greater cell degradation over time.

4.3.2.2. Battery pack configuration: 96S54P (secondary lightweighting). Given that the vehicle with the stearyl alcohol PCM-cooling system consumes 91.90 % of what the active liquid-cooled vehicle does, we decided to reduce the number of cells in the battery pack to match the capacity of approximately 91.90 % of the reference battery pack (and therefore the same range) in order to achieve a secondary lightweighting, resulting in about 149.11 Ah compared to the original 162.25 Ah. To accomplish this, we need about 54.2 cells in parallel (each cell having a capacity of 2.75 Ah). We opted for 54 cells in parallel, as done in the air-cooled configuration, rounding down to the nearest whole number. This new 96S54P configuration results in a weight reduction of 22.559 kg by removing 480 cells from the battery pack.

All simulations were then repeated, further reducing the vehicle's weight by the above-mentioned 22.559 kg. In the 96S54P battery pack configuration, the total mass of the PCM is 36.766 kg (see Table 4).

The total weight reduction is 74.674 kg, resulting in a final vehicle weight of approximately 1911.9 kg. The TEST model simulation was also repeated with the new motor torques and angular speeds, considering the average power consumed by the auxiliaries to be 681.5 W. New results were then obtained using the Simulink model of the battery pack.

Fig. 19 presents the results of a single battery pack simulation for the WLTC driving cycle, class 3b, starting from 80 % SOC and an initial battery pack temperature of 25 °C. In particular, Fig. 19a reports the battery current and the battery voltage during the entire simulation; Fig. 19b the battery SOC and the battery energy; Fig. 19c shows the battery temperature; and Fig. 19d the energy absorbed by the stearyl alcohol PCM during the phase change.

In this configuration, the average consumption on the WLTC cycle, class 3b, is equal to 32.23 kWh/(100 km), 91.73 % of the consumption of the active cooled vehicle, and only 0.85 % more than the same air-cooled vehicle model (96S54P). The range to discharge 80 % of the SOC of the battery pack corresponds to 148.6 km, only 0.22 % lower than the range of the active cooled vehicle, and only 0.84 % less than the same air-cooled vehicle model (96S54P). The PCM-cooled vehicle thus obtained, with 480 fewer cells,

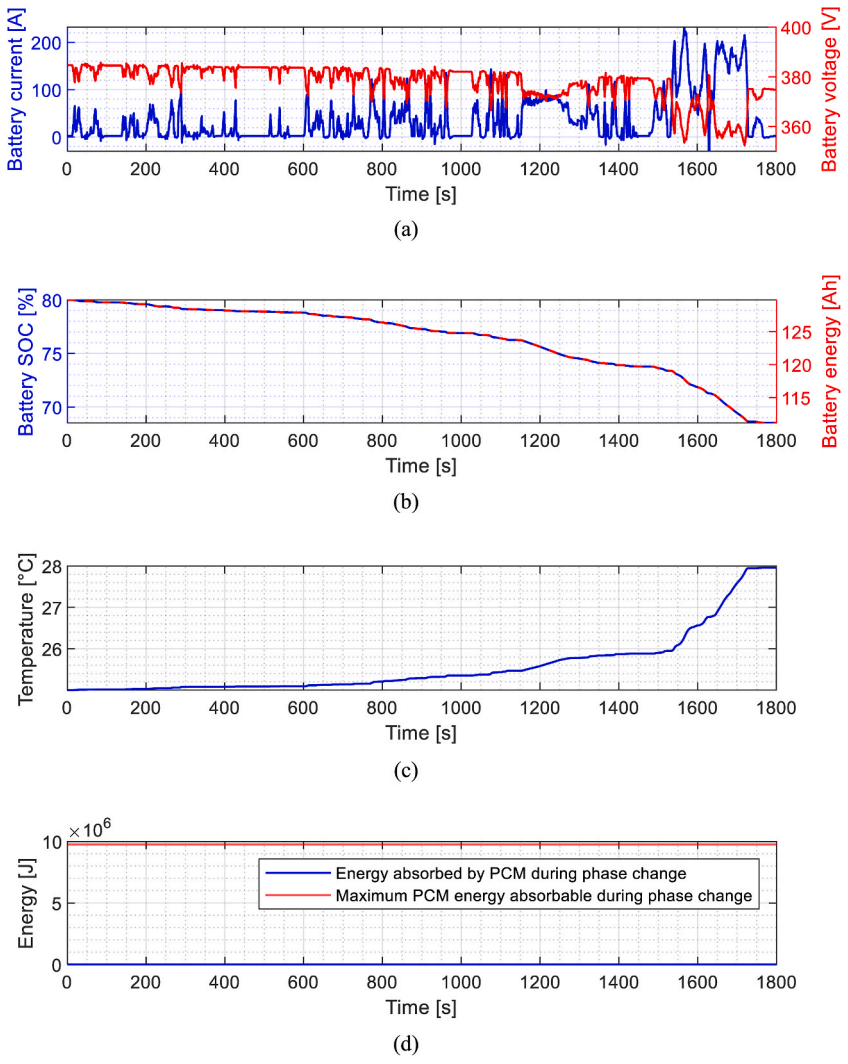

Fig. 17. Results for the vehicle with passive stearyl alcohol PCM cooled battery pack (96S59P). Results in terms of (a) battery current and battery voltage; (b) battery SOC and battery energy; (c) battery temperature; (d) energy absorbed by the stearyl alcohol PCM during the phase change.

has a range comparable to that of the active-cooled vehicle.

Now, also for this passive PCM cooled vehicle, different sets of simulations are presented, once again composed of the repetition of WLTC cycles (class 3b), starting from SOC equal to 100 % until the SOC drops below 20 % or until the battery temperature exceeds 60 °C. The results are reported in Fig. 20. As for the previous configuration without secondary lightweighting, the same assumptions as the previous case are made for the Q_{PCM} of the simulations from 57 °C as initial battery temperature and above. Even in Fig. 20, the vertical red lines separate one WLTC cycle from the next, while the horizontal green line in Fig. 20a represents the 20 % of SOC, and the dotted horizontal red line in Fig. 20b represents the maximum temperature limit, equal to 60 °C.

The observations on the battery state of charge are the same as for the air-cooled and glycol PCM configurations (see Fig. 20a and 20b).

As shown in Fig. 20b, simulation sets with initial battery pack temperatures up to 20 °C never reach the melting point of 57 °C. For sets starting from 25 °C to 50 °C, the battery pack reaches 57 °C and maintains this temperature until the end of the final simulation. In the sets starting from 55 °C to 57 °C, the battery pack temperature exceeds 57 °C in the final stages of the last simulation, as the PCM has completed its energy absorption for the phase change (see Fig. 20c). Lastly, the case starting from an initial battery pack temperature of 60 °C behaves similarly to air-cooled batteries, with the temperature continuously raising.

This solution, which is also suitable for private vehicles for daily use, has the same advantages and disadvantages as the previous configuration, but in this case a secondary lightweighting has also been achieved, followed by a further reduction in energy consumption.

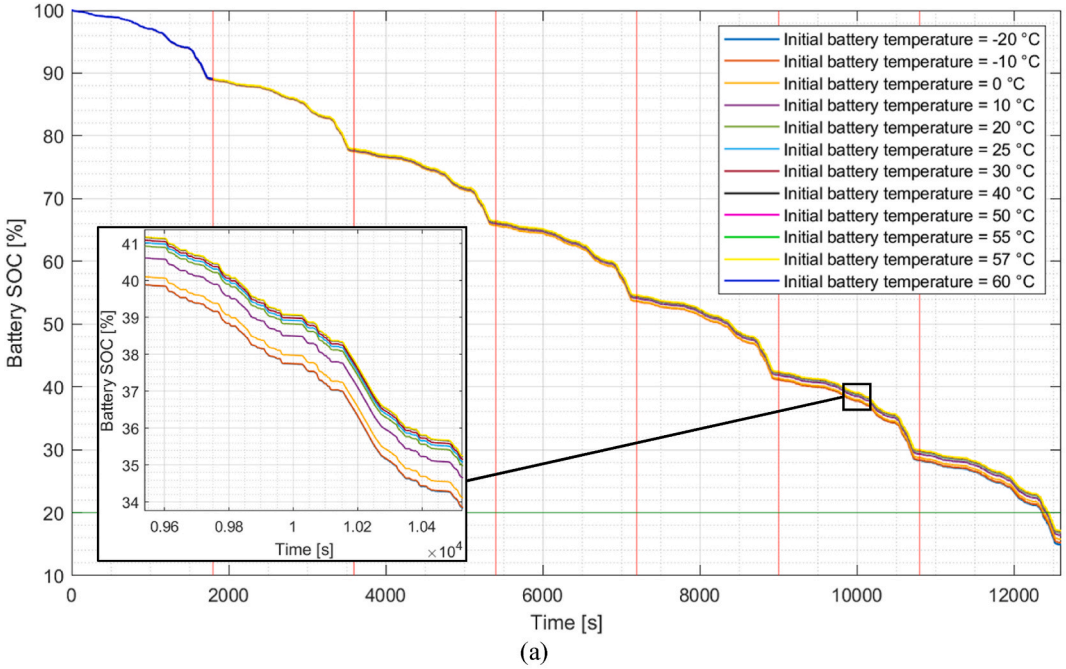

(a)

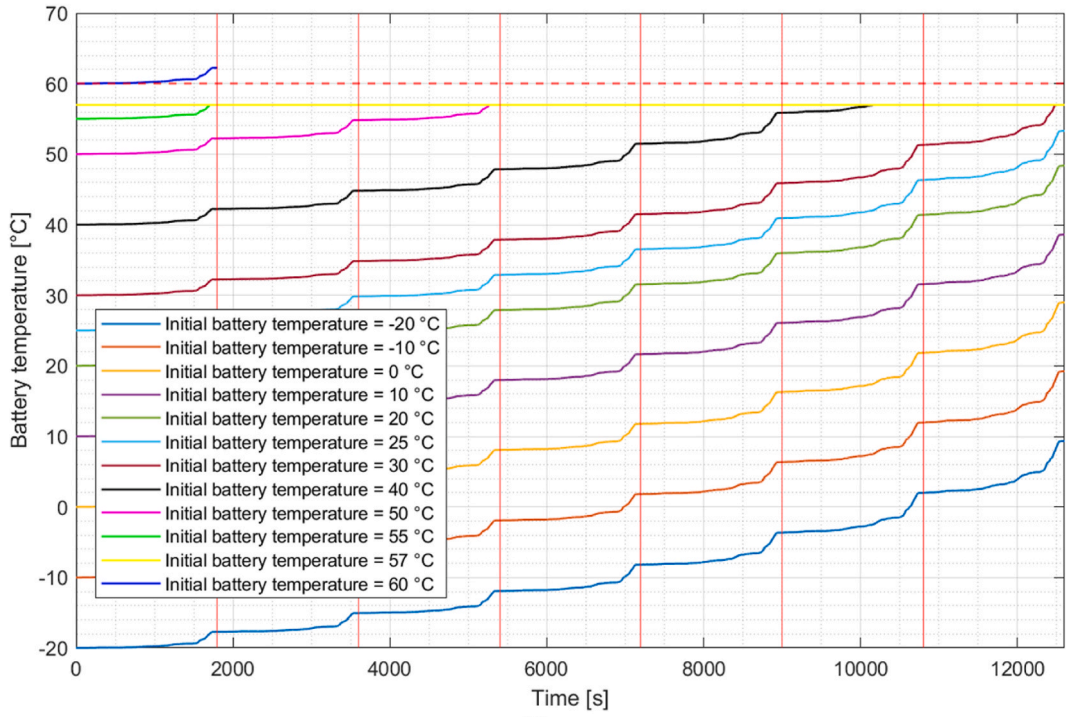

(b)

Fig. 18. WLTC repetitions for the vehicle with passive stearyl alcohol PCM cooled battery pack (96S59P). (a) battery SOC; (b) battery average temperature; and (c) energy absorbed by PCM during phase change.

5. Discussion

This section summarizes the main results presented in the previous section.

For the reference vehicle with the active liquid-cooling system, it has been found that during the WLTC (class 3b) driving cycle,

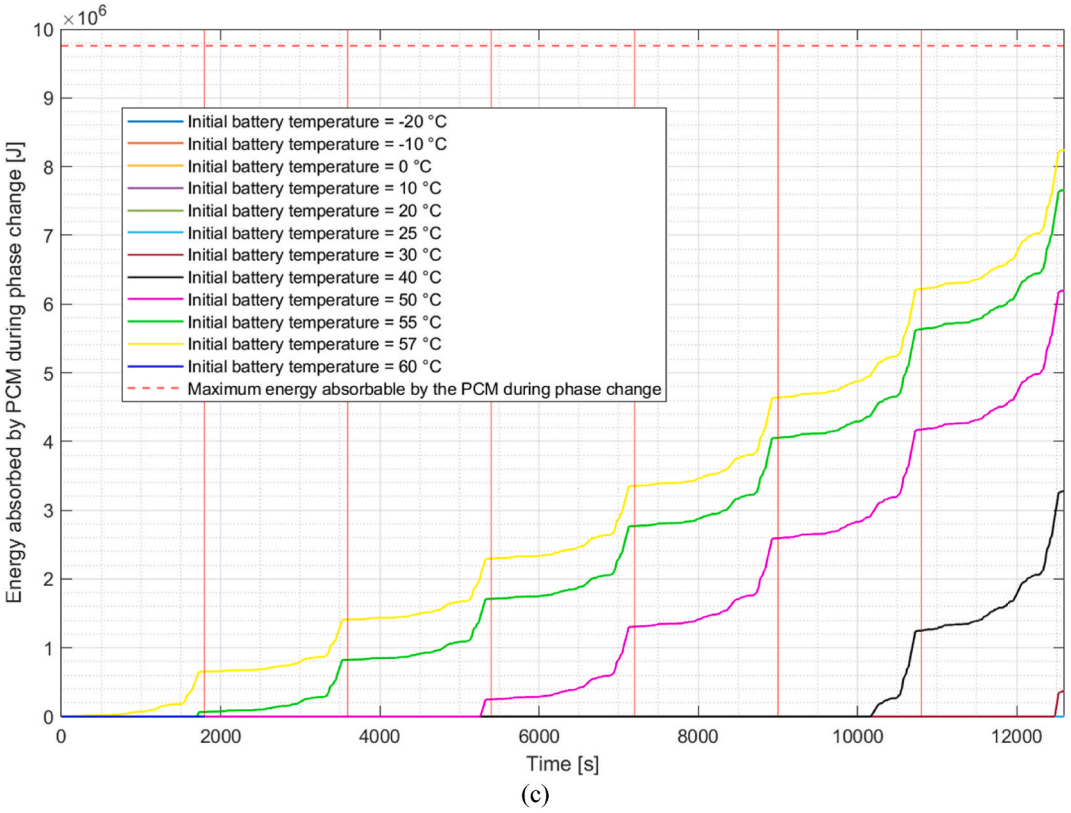

Fig. 18. (*continued*).

starting from different initial temperatures of the battery pack, the battery pack temperature tends to approach the refrigerant temperature of 20 °C. This helps maintain the battery pack's optimal operating temperature, thus limiting cell degradation.

Table 5 summarizes the key results obtained by reducing the vehicle weight using alternative battery pack cooling systems compared to the original active liquid-cooling system.

By using a passive air-cooling system, it is possible to obtain a 4.5 % reduction in weight compared to the reference vehicle and an 8.9 % consumption saving on WLTC (class 3b) driving cycle. In this way, an increase in range of 9.8 % is obtained, which allows for a secondary lightweighting by reducing the capacity of the battery pack and therefore its number of cells (from 5664 to 5184, from configuration 96S59P to 96S54P). This secondary lightweighting allows the weight of the reference vehicle to be lightened by a further 1.1 %, for a total of 5.6 % lightweighting, while consumption remains comparable with the case of the air-cooled vehicle without reducing the number of battery cells.

For air-cooled configurations, starting from an initial temperature of the battery pack from −20 °C up to 30 °C, carrying out a series of non-stop repetitions of the WLTC cycle (class 3b), what limits the vehicle is the capacity of the battery pack (i.e. reaching the minimum SOC threshold set to 20 %), while for the simulations starting from a battery pack of 40 °C and above, reaching the upper battery pack temperature limit of 60 °C is the limiting factor. In fact, 60 °C is the maximum allowable operation temperature of the battery pack considered. This air-cooled system therefore is well suited to operating environments where the battery pack does not exceed approximately 30 °C before starting the vehicle. Therefore, for extreme temperature conditions, the passive air-cooled system is well suited only to vehicles operating in fleets with programmable and predefined missions. Furthermore, the battery pack cells may experience faster degradation than the actively liquid-cooled configuration, as they do not always operate around the optimal temperature of 20 °C. This last aspect could therefore be studied and explored deeper in a future study.

By using a passive glycerol PCM-based cooling system, it is possible to obtain a 1.3 % reduction in weight and an 7.6 % saving in consumption, on WLTC (class 3b) driving cycle. In this way, an increase in range of 8.3 % is obtained, which allows for a secondary lightweighting by reducing the capacity of the battery pack and therefore its number of cells (from 96S59P to 96S54P). This secondary lightweighting allows for a total vehicle lightweighting of 2.7 %.

For glycerol PCM-cooled configurations, performing a series of continuous WLTC cycle (class 3b) repetitions, starting with an initial battery pack temperature below 0 °C, the temperature never reaches 26 °C, the melting point of glycerol PCM. When starting from 0 to 25 °C, the battery pack reaches 26 °C and maintains this temperature until the SOC drops to 20 %. Above 26 °C, the temperature trend is similar to the air-cooled configurations, and the limiting factor becomes reaching the 60 °C threshold. This glycerol PCM-cooled system is thus well-suited for environments where the battery pack does not exceed approximately 30 °C before vehicle operation, suitable for vehicles working in fleets with controlled and programmed mission conditions. The advantage of this solution is

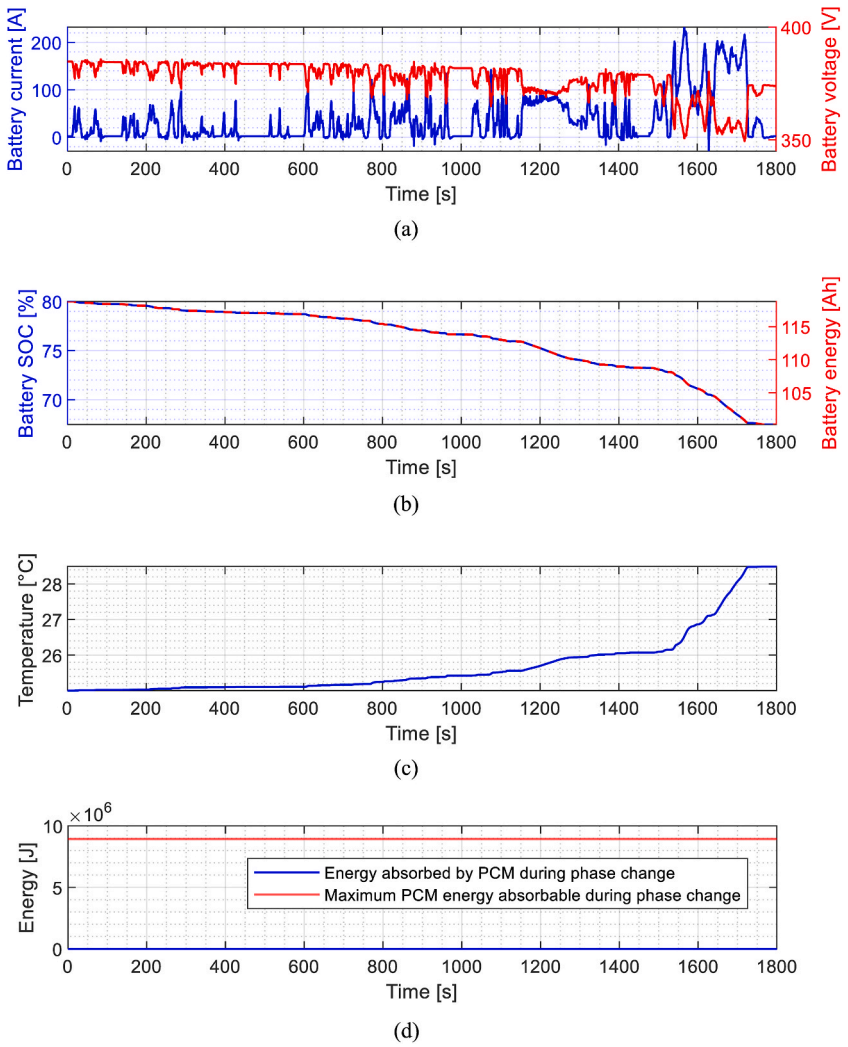

Fig. 19. Results for the vehicle with passive stearyl alcohol PCM cooled battery pack (96S54P). Results in terms of (a) battery current and battery voltage; (b) battery SOC and battery energy; (c) battery temperature; (d) energy absorbed by the stearyl alcohol PCM during the phase change.

maintaining an optimal battery temperature for initial temperatures below 26 °C, reducing cell degradation over time. Glycerol PCM offers similar characteristics to passive air cooling but with improved temperature maintenance around optimal conditions for initial temperatures below 26 °C.

To avoid fleet-specific use with predefined missions, stearyl alcohol PCM with a melting point of 57 °C can be considered instead. This PCM can achieve a 2.4 % weight reduction and an 8.1 % consumption saving on the WLTC (class 3b) driving cycle, resulting in an 8.8 % range increase compared to the baseline vehicle. This allows for secondary lightweighting by reducing the battery pack capacity and the number of cells (from 96S59P to 96S54P), leading to a total vehicle lightweighting of 3.8 %.

For the stearyl alcohol PCM-cooled battery pack in the 96S59P configuration, performing continuous WLTC cycle repetitions with initial battery pack temperatures up to 25 °C, the pack does not reach the 57 °C melting point of the PCM. Starting from 30 to 57 °C, the battery pack reaches and maintains 57 °C until the SOC drops below 20 %. For the 96S54P configuration, starting from up to 20 °C the battery pack does not reach the PCM melting point. From 25 to 50 °C, the battery pack reaches 57 °C and maintains it until the SOC drops below 20 %. Starting from 55 to 57 °C, in the final stages of the last WLTC cycle (before reaching 20 % SOC), the battery pack exceeds 57 °C as the PCM completes the energy absorption for the phase change but does not exceed 60 °C.

Therefore, the vehicle with a stearyl alcohol PCM cooling system, with a melting point of 57 °C, is suitable for daily use and not just for fleet operations as long as the initial battery pack temperature does not exceed 57 °C. The advantage of this solution is keeping the battery pack below 60 °C even when starting from high temperatures. However, compared to the glycerol PCM with a 26 °C melting point, it does not maintain the battery pack in an optimal temperature range, potentially leading to greater cell degradation over time.

By adopting the battery pack cooling system replacement technique, it was possible to achieve a total vehicle lightweighting of between approximately 27 kg and about 111 kg. In particular, approximately 27 kg of weight reduction was obtained by replacing the

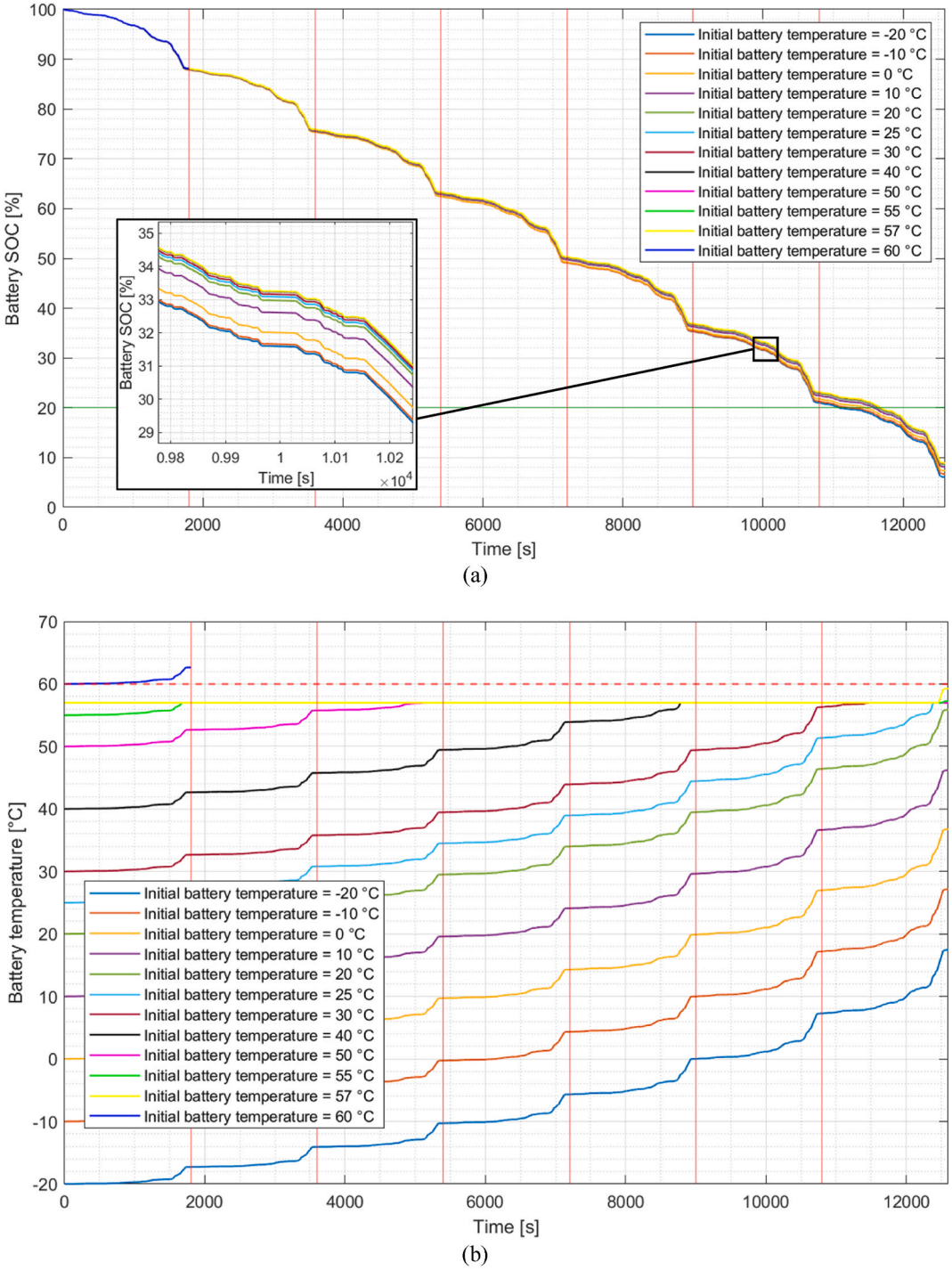

Fig. 20. WLTC repetitions for the vehicle with passive stearyl alcohol PCM cooled battery pack (96S54P). (a) battery SOC; (b) battery average temperature; and (c) energy absorbed by PCM during phase change.

liquid cooling system with one based on glycerol PCM, undertaking only a primary lightweighting. Instead, by replacing the liquid system with an air-cooled one and implementing a secondary lightweighting (by reducing the battery pack capacity), it was possible to achieve a total weight reduction of approximately 111 kg.

The lightweighting obtained can be considered not significant if compared to that obtained by other studies. For example, Magna International and Ford Motor Company, for a project of the United States Department of Energy achieved a weight saving of 364 kg for a five-passenger sedan car [54].

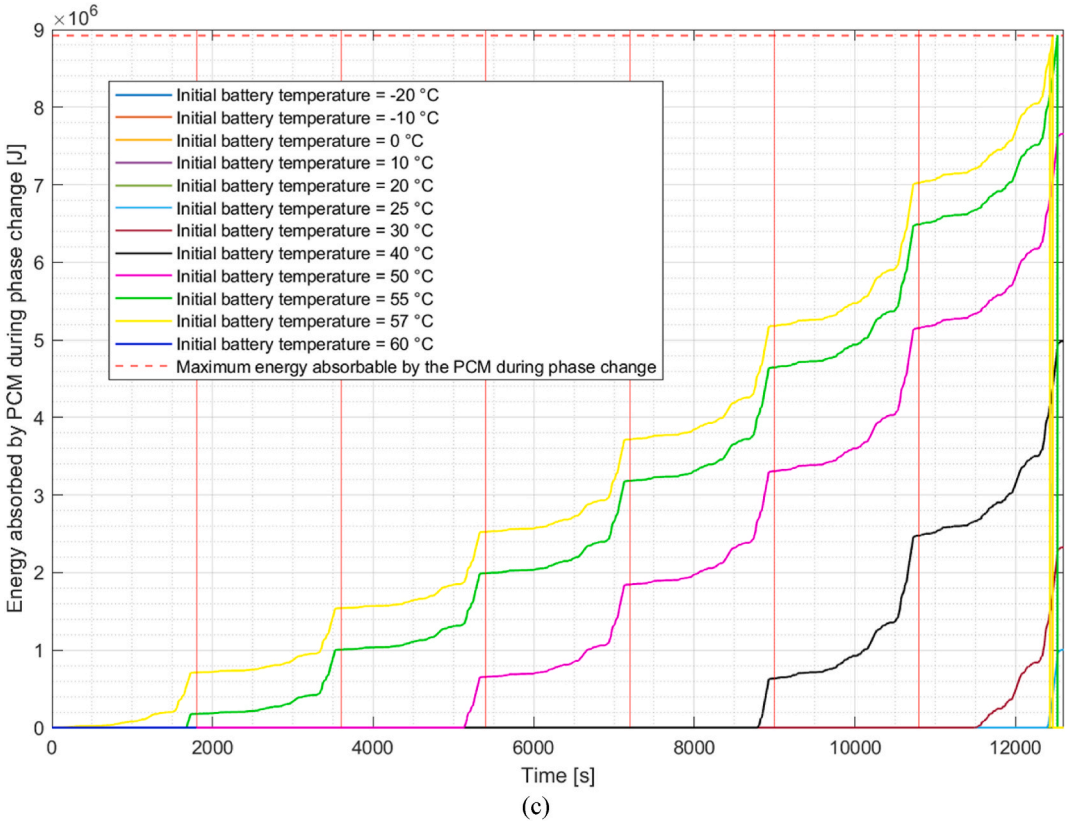

Fig. 20. (*continued*).

Table 5
Results. Resume of the main results of the study.

Battery pack system	Cooling system weight [kg]	Primary lightweighting [kg]	Secondary lightweighting [kg]	Total weight reduction [kg]	Lightweighting [%]	Energy consumption [kWh/100 km]	Range [km]
Active cooled 96S59P	88.84	–	–	–	0	35.13	149.0
Air cooled 96S59P	–	88.84	–	88.84	4.5	31.99	163.6
Air cooled 96S54P	–	88.84	22.56	111.40	5.6	31.96	149.9
Glycerol 96S59P	62.30	26.54	–	26.54	1.3	32.45	161.3
Glycerol 96S54P	57.02	31.82	22.56	54.42	2.7	32.39	147.9
Stearyl alcohol 96S59P	40.17	48.67	–	48.67	2.4	32.28	162.1
Stearyl alcohol 96S54P	36.77	52.07	22.56	74.67	3.8	32.23	148.6

Furthermore, in study [55], two different lightweights were considered, achievable by the partial replacement of conventional iron and steel components with similar components made of aluminium. A weight reduction of 140 kg was obtained considering the current trend of increasing use of aluminium for automotive components. Then, it was also considered a drastic reduction of 300 kg.

Despite this, a weight reduction of between 27 and 111 kg by acting on a single component of the vehicle is still interesting. In fact, in Ref. [56], a weight saving of 5.5 kg was achieved for a single front axle of a light truck. This is to indicate how even a small contribution to weight reduction can be significant, especially if applied in conjunction with other lightweighting techniques on other vehicle components.

Finally, it is possible to cite a further study, in line with the lightweighting results obtained by replacing the battery pack cooling

system, the study [57]. The latter states that for a mid-size car, using forging as a manufacturing technique it is possible to obtain a weight reduction of 42 kg in powertrain and chassis components. While, for a light commercial vehicle it is possible to obtain a lightweighting of 99 kg.

6. Conclusion

This study evaluates the possibility of the vehicle lightweighting by acting on the battery pack, and in particular on its thermal management system. A feasibility study was then carried out regarding the replacement of an active liquid cooling system with different passive systems: air-cooled and cooling systems based on PCM materials.

In this paper, the virtual model of a sedan car equipped with a 96S59P battery pack configuration (96 cells in series and 59 in parallel), featuring an active liquid-cooling system weighing 88.84 kg and consuming an average power of 815.5 W to maintain the refrigerant at approximately 20 °C, was used as the baseline vehicle. This reference car was firstly compared to an equivalent vehicle, but using a battery pack cooled by a passive air system and then with a vehicle using two different PCM-based (Phase Change Material) cooling systems: glycerol PCM and stearyl alcohol PCM. For each vehicle, the primary lightweighting achieved by changing the battery pack cooling system was evaluated first, followed by the secondary lightweighting obtained by reducing the number of cells in the battery pack to restore the original range of the baseline vehicle.

For this study, the reference driving cycle is the standard WLTC, and the vehicle motor torque and angular speed time history is obtained through VI-CarRealTime simulations on this cycle. Then, VI outputs were used as input to a consolidated vehicle longitudinal dynamics simulation tool to obtain the power demand that the vehicle system requires from the battery pack. Finally, the different battery thermal management systems are studied using an ad hoc Simulink model.

By using a passive air-cooling system, the primary lightweighting is achieved by eliminating the approximately 90 kg of active system. While for the PCM systems it is necessary to consider the additional weight given by the PCM itself, so it is possible to obtain a lower lightweighting: about 27 kg of lightweighting for glycerol PCM and about 49 kg for stearyl alcohol. Vehicles thus lightened have lower energy consumption and so a range that is more than 10 km longer on the WLTC standard cycle. For all the vehicle configuration with passive cooling systems, to bring the vehicle range back to around 150 km, it is sufficient to reduce the battery pack by 5 cells in parallel, for a total of 480 cells and 22 and a half kilos removed. This results in a secondary lightweighting of 22 and a half kilos for the passive air-cooling system, while a higher secondary lightweighting is obtained for the PCM systems, also taking into account the smaller quantity of PCM required. In this way, it is possible to obtain a total lightweighting of more than one percentage point more than in each case with only primary lightweighting.

From this study it emerged that an air-cooled system leads to greater lightweighting, but it is only suitable for vehicle fleets, and it leads the battery pack to operate at non-optimal temperatures, with consequent degradation of the cells. A passive glycerol PCM system, with its 26 °C melting point, can allow the battery pack to operate near its optimal operating temperature, limiting cell degradation. But this system is still only applicable to fleets. The stearyl alcohol PCM system can instead be adopted for private vehicles, avoiding overheating thanks to its 57 °C melting point. But, in this case, the problem of cell degradation remains.

This study demonstrated the feasibility of replacing the active liquid cooling system of the battery pack with different solutions, showing for each the advantages (large weight reduction with a passive air system, maintaining the battery pack operation close to its optimal temperature using a glycerol PCM system) and the limitations (higher cell degradation for air-cooled and stearyl alcohol-cooled systems, fleet-only application for air-cooled and glycerol-cooled systems). The aim of this work is in fact a feasibility study and not an accurate thermal management modelling. The next steps could then be the choice of a specific configuration and the creation of a more accurate battery and thermal management model, in order to be able to adopt it for a real design phase.

CRediT authorship contribution statement

Giulia Sandrini: Writing – review & editing, Writing – original draft, Validation, Software, Methodology, Formal analysis, Data curation, Conceptualization. **Daniel Chindamo:** Writing – review & editing, Visualization, Supervision, Project administration, Methodology, Conceptualization. **Marco Gadola:** Writing – review & editing, Visualization, Supervision, Project administration. **Andrea Candela:** Data curation. **Paolo Magri:** Data curation.

Data availability statement

The data presented in this study are available on request from the corresponding author. The data are not publicly available due to University of Brescia privacy policy.

Funding

This research is funded by the European Union, NextGenerationEU, see below.

Declaration of competing interest

The authors declare that they have no known competing financial interests or personal relationships that could have appeared to influence the work reported in this paper.

Acknowledgements

This study was financed by the European Union—NextGenerationEU (National Sustainable Mobility Center CN00000023, Italian Ministry of University and Research Decree n. 1033–17/06/2022, Spoke 11—Innovative Materials & Lightweighting). The opinions expressed are those of the authors only and should not be considered as representative of the European Union or the European Commission's official position. Neither the European Union nor the European Commission can be held responsible for them. CUP D83C22000690001.

Appendix A

Nomenclature

Abbreviation	Description
°C	Celsius degree, plural Celsius degreed, unit of measure of the temperature (1 °C is equal to about 273.15K)
A	Ampere, unit of measure (SI) of the electrical current
Ah	Ampere hour, plural Ampere hours, unit of measure of the nominal capacity of a battery pack or of a cell of the battery pack, where A is the unit of measure (SI) of the electrical current, and h is the unit of measure of the time (1h = 3600s)
ALMMII	American Lightweight Materials Manufacturing Innovation Institute
$C_3H_8O_3$	Glycerol
C_{bat}	Battery pack energy
C_{bat_kWh}	Nominal battery pack capacity
C_{cell_nom}	Rated capacity of the battery cell at nominal temperature
C_{cell}	Energy of the single cell of the battery pack
C_h	Battery heat coefficient
C_{kWh}	Battery power storage
CNR	National (Italian) Research Council
Cons	Energy consumption
$c_{p.bat}$	Specific heat capacity of the battery cell
dt	Step simulation time
ERV	Energy Reduction Value
FRV	Fuel Reduction Value
h	Hour, plural hours, unit of measure of the time (1h = 3600s)
I_{bat}	Battery pack current
J	Joule, unit of measure (SI) of the energy, 1J = 1Nm = 1 kg m^2/s^2
J/kg	Joule per kilogram, unit of measure (SI) of the latent heat
JLR	Jaguar Land Rover
K	Kelvin, unit of measure (SI) of the temperature
K_{CP}	Heat conductance at the cooling plate
kg	Kilogram, plural kilogramme, unit of measure (SI) of the mass
kg•m^2	Unit of measure (SI) of the moment of the inertia
kg•m^{-3}	Unit of measure (SI) of the density
kg/m^3	Unit of measure (SI) of the density
km	Kilometre, plural kilometres, unit of measure (SI) of the length/distance, 1 km = 1000m
km/h	Kilometres per hour, unit of measure of the speed, commonly adopted in the automotive field
kJ•kg^{-1}•K^{-1}	Unit of measure (SI) of the specific heat capacity (where 1 kJ = 1000J)
$kJ/kg \bullet K$	Unit of measure (SI) of the specific heat capacity (where 1 kJ = 1000J)
kW	Kilowatt, plural kilowatts, unit of measure (SI) of the power, 1 kW = 1000W
kW/°C	Unit of measure of the heat conductance (where 1 kW = 1000W, and 1 °C is equal to about 273.15K)
kWh	Unit of measure used to express the capacity of a battery pack or of a cell of the latter in the form of energy, where kW is the unit of measure (SI) of the power, and h is the unit of measure of the time (1h = 3600s)
kWh/100 km	Unit of measure of the energy consumption every 100 km, commonly adopted in the automotive sector (where 1 kW = 1000W, 1h = 3600s, and 1 km = 1000m)
kWh/(100 km • 100 kg)	Unit of measure of the energy consumption every 100 km every 100 kg of vehicle mass reduction, commonly adopted for the ERV index in the automotive sector, to evaluate the vehicle lightweighting (where 1 kW = 1000W, 1h = 3600s, and 1 km = 1000m)
L	Litre, plural litres, unit of measure of volume, 1L = 0.001m^3
L/(100 km • 100 kg)	Unit of measure of the fuel consumption every 100 km every 100 kg of vehicle mass reduction, commonly adopted for the FRV index in the automotive sector, to evaluate the vehicle lightweighting (where 1L = 0.001m^3, and 1 km = 1000m)
LCA	Life Cycle Assessment
LIB	Lithium-Ion Battery
L_{PCM}	Latent heat of the PCM
m	Metre, plural metres, unit of measure (SI) of the length/distance
m^2	Square metre, plural square metres, unit of measure (SI) of the surface/area
m^3	Cube metre, plural cube metres, unit of measure (SI) of the volume
MOST	National (Italian) Center for Sustainable Mobility
m_{PCM}	PCM mass related to the single cell of the battery pack
N	Newton, unit of measure (SI) of the force, 1N = 1 kg m/s^2
NCA	Nickel–cobalt–aluminium
Nm	Newton metre, plural Newton metres, unit of measure (SI) of the mechanical torque

(*continued on next page*)

(*continued*)

N_p	Number of cells in parallel in the battery pack
N_s	Number of cells in series in the battery pack
OCV	Open Circuit Voltage
P_{bat}	Battery pack network power
PCM	Phase Change Material
P_{demand}	Power demand
PERD	Program of Energy Research and Development
P_{loss}	Battery network power loss
Q_{bat}	Heat generated by the batteries
Q_{CP}	Cooling heating power of the cooling plate of the thermal management system
Q_{PCM}	Maximum energy absorbed by the PCM during the change of state
Range	Theoretical range of the vehicle, to ideally discharge the battery pack from 100 % to zero SOC
$Range_{80\%}$	Vehicle range, to discharge the battery pack from 100 % to 20 % SOC
RPM	Round per minute, plural rounds per minute, unit of measure of the angular speed, commonly adopted in the automotive field for the rotational speed of motors/engines, 1RPM = $2\pi/(60s)$
s	Second, plural seconds, unit of measure (SI) of the time
SI	International System of Units
SOC	State of Charge
SOC_{init}	Initial battery State of Charge, at the start of the simulation
s_{WLTC}	Distance travelled by the vehicle on the WLTP cycle, class 3b
T_{bat_init}	Initial battery pack temperature, at the start of the simulation
T_{bat_prev}	Battery temperature at the instant of calculation prior to the one considered
T_{CP}	Average temperature of the refrigerant flowing in the heat exchangers
TEST	Target-speed EV (Electric Vehicle) Simulation Tool
U.S.	United States
V	Volt, plural Volts, unit of measure (SI) of voltage (or electric potential, or potential difference)
v_{bat}	Total volume of the battery cells
V_{bat}	Battery pack voltage
V_{bat_prev}	Battery pack voltage at the instant of calculation prior to the one considered
v_{cell}	Volume of a single battery cell
VI-CRT	VI-CarRealTime
W	Watt, plural Watts, unit of measure (SI) of the power, 1W = 1 J/s
WHF	Downforce coefficient
WLTC	Worldwide Harmonized Light-Duty Vehicles Test Cycle
WLTP	Worldwide Harmonized Light-Duty Vehicles Test Procedure
WMG	Warwick Manufacturing Group
ΔSOC	Difference between the battery SOC at the beginning and end of the simulation
ρ_{bat}	Average density of the battery cell
σ	Ratio of the battery power output (kW) multiplied by 1 h and the battery power storage (kWh)
Ωm	Ohm metre, plural Ohm metres, unit of measure (SI) of the cable specific resistivity
Ω	Ohm, unit of measure (SI) of the electrical resistance, 1Ω = 1V/A

Appendix B

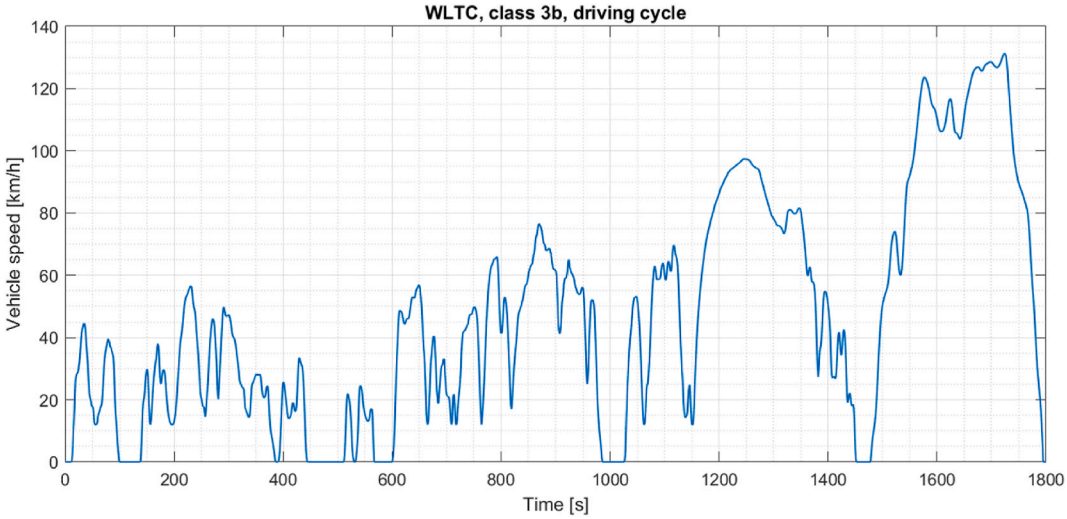

Fig. B1. WLTC cycle. Speed profile of the WLTC (Worldwide Harmonized Light-Duty Vehicles Test Cycle), class 3b, driving cycle, related to the WLTP (Worldwide Harmonized Light-Duty Vehicles Test Procedure) [38].

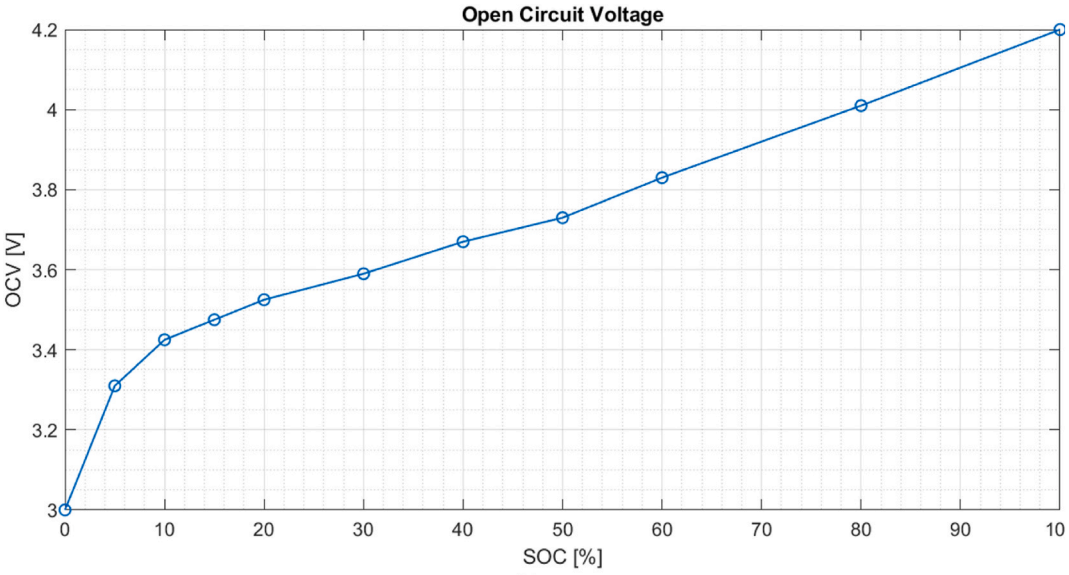

(a)

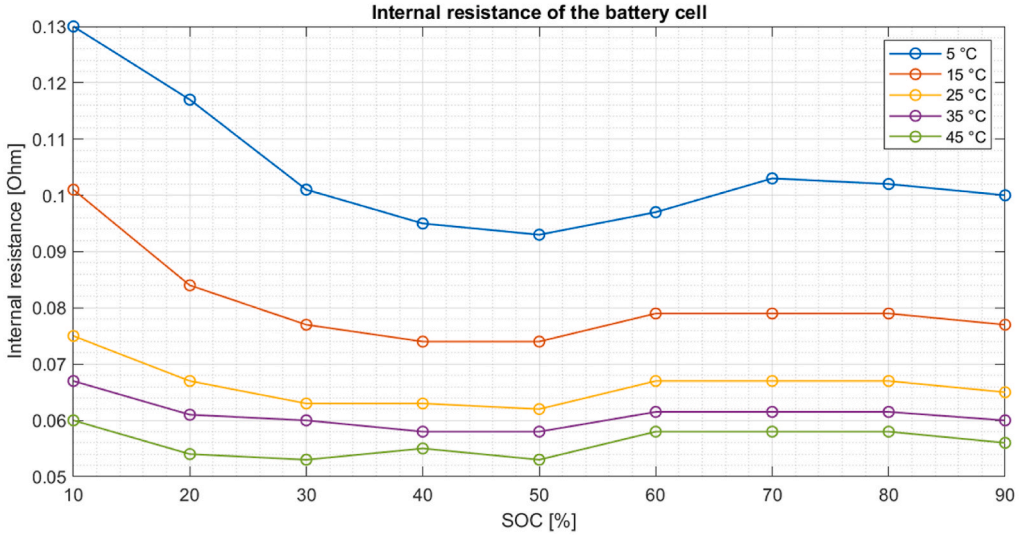

(b)

Fig. B2. Cell OCV and internal resistance. (a) Open Circuit Voltage (OCV) of the single cell in function of the battery State of Charge (SOC) [49]; (b) Internal resistance of the single battery cell, in function of the battery State of Charge (SOC) and of the battery temperature [50].

References

[1] European Parliament and Council of the European Union, Ordinary legislative procedure 2021/0197(COD), in: https://oeil.secure.europarl.europa.eu/oeil/popups/ficheprocedure.do?reference=2021/0197(COD)&l=en, 2023. (Accessed 8 January 2024).
[2] G. Sandrini, D. Chindamo, M. Gadola, Regenerative braking logic that Maximizes energy recovery ensuring the vehicle stability, Energies 15 (2022) 5846, https://doi.org/10.3390/en15165846.
[3] G. Sandrini, M. Gadola, D. Chindamo, P. Magri, Efficient regenerative braking strategy aimed at preserving vehicle stability by preventing wheel locking, Transport. Res. Procedia 70 (2023) 28–35, https://doi.org/10.1016/j.trpro.2023.10.005.
[4] H. Monteiro, R. Alonso, M. Gonçalves, M. Iten, N.S. Caetano, Life cycle energy of vehicles on lightweighting and alternative powertrain strategies—a review, Energy Rep. 8 (2022) 241–247, https://doi.org/10.1016/j.egyr.2022.01.037.
[5] G.M. Lewis, C.A. Buchanan, K.D. Jhaveri, J.L. Sullivan, J.C. Kelly, S. Das, A.I. Taub, G.A. Keoleian, Green principles for vehicle lightweighting, Environ. Sci. Technol. 53 (2019) 4063–4077, https://doi.org/10.1021/acs.est.8b05897.
[6] A. Candela, G. Sandrini, M. Gadola, D. Chindamo, P. Magri, Lightweighting in the automotive industry as a measure for energy efficiency: review of the main materials and methods, Heliyon 10 (2024) e29728, https://doi.org/10.1016/j.heliyon.2024.e29728.
[7] F. Czerwinski, Current trends in automotive lightweighting strategies and materials, Materials 14 (2021) 6631, https://doi.org/10.3390/ma14216631.

[8] A. Cimprich, K. Sadayappan, S.B. Young, Lightweighting electric vehicles: scoping review of life cycle assessments, J. Clean. Prod. 433 (2023) 139692, https://doi.org/10.1016/j.jclepro.2023.139692.
[9] S. Das, D. Graziano, V.K.K. Upadhyayula, E. Masanet, M. Riddle, J. Cresko, Vehicle lightweighting energy use impacts in U.S. light-duty vehicle fleet, Sustain. Mater. Technol. 8 (2016) 5–13, https://doi.org/10.1016/j.susmat.2016.04.001.
[10] Warwick, WMG Part of a £37m Project to Develop Lightweight Vehicles, 2018 n.d. https://warwick.ac.uk/newsandevents/pressreleases/wmg_part_of_a_37m_project_to_develop_lightweight_vehicles1/. April 18, 2024
[11] MOST, Centro Nazionale per la Mobilità Sostenibile. https://www.centronazionalemost.it/. (Accessed 8 July 2024).
[12] C. Spreafico, Can modified components make cars greener? A life cycle assessment, J. Clean. Prod. 307 (2021) 127190, https://doi.org/10.1016/j.jclepro.2021.127190.
[13] G. Giordano, Plastics power a new generation of electric vehicles, Plast. Eng. 75 (2019) 24–33, https://doi.org/10.1002/peng.20182.
[14] V.K.K. Upadhyayula, A.G. Parvatker, A. Baroth, K. Shanmugam, Lightweighting and electrification strategies for improving environmental performance of passenger cars in India by 2030: a critical perspective based on life cycle assessment, J. Clean. Prod. 209 (2019) 1604–1613, https://doi.org/10.1016/j.jclepro.2018.11.153.
[15] J.M. Luk, H.C. Kim, R.D. De Kleine, T.J. Wallington, H.L. MacLean, Greenhouse gas emission benefits of vehicle lightweighting: Monte Carlo probabalistic analysis of the multi material lightweight vehicle glider, Transp Res D Transp Environ 62 (2018) 1–10, https://doi.org/10.1016/j.trd.2018.02.006.
[16] F. Del Pero, M. Delogu, L. Berzi, C.A. Dattilo, G. Zonfrillo, M. Pierini, Sustainability assessment for different design solutions within the automotive field, Procedia Struct. Integr. 24 (2019) 906–925, https://doi.org/10.1016/j.prostr.2020.02.080.
[17] C. Koffler, K. Rohde-Brandenburger, On the calculation of fuel savings through lightweight design in automotive life cycle assessments, Int. J. Life Cycle Assess. 15 (2010) 128–135, https://doi.org/10.1007/s11367-009-0127-z.
[18] H.C. Kim, T.J. Wallington, Life cycle assessment of vehicle lightweighting: a physics-based model to estimate use-phase fuel consumption of electrified vehicles, Environ. Sci. Technol. 50 (2016) 11226–11233, https://doi.org/10.1021/acs.est.6b02059.
[19] H.C. Kim, T.J. Wallington, J.L. Sullivan, G.A. Keoleian, Life cycle assessment of vehicle lightweighting: novel mathematical methods to estimate use-phase fuel consumption, Environ. Sci. Technol. 49 (2015) 10209–10216, https://doi.org/10.1021/acs.est.5b01655.
[20] F. Del Pero, M. Delogu, M. Pierini, The effect of lightweighting in automotive LCA perspective: estimation of mass-induced fuel consumption reduction for gasoline turbocharged vehicles, J. Clean. Prod. 154 (2017) 566–577, https://doi.org/10.1016/j.jclepro.2017.04.013.
[21] M. Delogu, F. Del Pero, M. Pierini, Lightweight design solutions in the automotive field: environmental modelling based on fuel reduction value applied to diesel turbocharged vehicles, Sustainability 8 (2016) 1167, https://doi.org/10.3390/su8111167.
[22] F. Del Pero, L. Berzi, A. Antonacci, M. Delogu, Automotive lightweight design: simulation modeling of mass-related consumption for electric vehicles, Machines 8 (2020) 51, https://doi.org/10.3390/machines8030051.
[23] G. Sandrini, M. Gadola, D. Chindamo, A. Candela, P. Magri, Exploring the impact of vehicle lightweighting in terms of energy consumption: analysis and simulation, Energies 16 (2023) 5157, https://doi.org/10.3390/en16135157.
[24] G. Sandrini, D. Chindamo, M. Gadola, A. Candela, P. Magri, Exploring the impact of vehicle lightweighting in terms of energy consumption: analysis and simulation on real driving cycle, Energies 17 (2024) 6398, https://doi.org/10.3390/en17246398.
[25] G. Sandrini, B. Có, G. Tomasoni, M. Gadola, D. Chindamo, The environmental performance of traction batteries for electric vehicles from a life cycle perspective, Environ. Climate Technol. 25 (2021), https://doi.org/10.2478/rtuect-2021-0053.
[26] Y. Lai, W. Wu, K. Chen, S. Wang, C. Xin, A compact and lightweight liquid-cooled thermal management solution for cylindrical lithium-ion power battery pack, Int. J. Heat Mass Tran. 144 (2019) 118581, https://doi.org/10.1016/j.ijheatmasstransfer.2019.118581.
[27] L. Sheng, H. Zhang, H. Zhang, L. Su, Z. Zhang, Lightweight liquid cooling based thermal management to a prismatic hard-cased lithium-ion battery, Int. J. Heat Mass Tran. 170 (2021) 120998, https://doi.org/10.1016/j.ijheatmasstransfer.2021.120998.
[28] Z. Tang, Z. Liu, J. Li, J. Cheng, A lightweight liquid cooling thermal management structure for prismatic batteries, J. Energy Storage 42 (2021) 103078, https://doi.org/10.1016/j.est.2021.103078.
[29] L. Zhou, S. Li, A. Jain, G. Chen, D. Guo, J. Kang, Y. Zhao, Lithium battery thermal management based on lightweight stepped-channel liquid cooling, J. Electrochem. Energy Convers. Storage (2024) 21, https://doi.org/10.1115/1.4063848.
[30] R. Youssef, T. Kalogiannis, H. Behi, A. Pirooz, J. Van Mierlo, M. Berecibar, A comprehensive review of novel cooling techniques and heat transfer coolant mediums investigated for battery thermal management systems in electric vehicles, Energy Rep. 10 (2023) 1041–1068, https://doi.org/10.1016/j.egyr.2023.07.041.
[31] R. Zhao, J. Gu, J. Liu, Optimization of a phase change material based internal cooling system for cylindrical Li-ion battery pack and a hybrid cooling design, Energy 135 (2017) 811–822, https://doi.org/10.1016/j.energy.2017.06.168.
[32] L.K. Singh, R. Kumar, A.K. Gupta, A.K. Sharma, S. Panchal, Computational study on hybrid air-PCM cooling inside lithium-ion battery packs with varying number of cells, J. Energy Storage 67 (2023) 107649, https://doi.org/10.1016/j.est.2023.107649.
[33] Y.S. Ranjbaran, M.H. Shojaeefard, G.R. Molaeimanesh, Thermal performance enhancement of a passive battery thermal management system based on phase change material using cold air passageways for lithium batteries, J. Energy Storage 68 (2023) 107744, https://doi.org/10.1016/j.est.2023.107744.
[34] S. Shahid, M. Agelin-Chaab, Development and analysis of hybrid cooling concepts for an electric battery pack, J. Energy Storage 73 (2023) 108952, https://doi.org/10.1016/j.est.2023.108952.
[35] G. Sandrini, D. Chindamo, M. Gadola, A. Candela, P. Magri, Primary and Secondary Vehicle Lightweighting Achieved by Acting on the Battery Thermal Management System. https://doi.org/10.1007/978-3-031-70392-8_44, 2024.
[36] D. Chindamo, M. Gadola, E. Bonera, P. Magri, Sensitivity of racing tire sliding energy to major setup changes: an estimate based on standard sensors, Energies 14 (2021) 5118, https://doi.org/10.3390/en14165118.
[37] M. Gadola, D. Chindamo, P. Magri, G. Sandrini, Analyzing porpoising on high downforce race cars: causes and possible setup adjustments to avoid it, Energies 15 (2022) 6677, https://doi.org/10.3390/en15186677.
[38] European Parliament and Council, Commission regulation (EU) 2017/1151. https://eur-lex.europa.eu/legal-content/EN/TXT/?uri=CELEX:32017R1151, 2017. (Accessed 2 October 2024).
[39] G. Sandrini, M. Gadola, D. Chindamo, Longitudinal dynamics simulation tool for hybrid apu and full electric vehicle, Energies 14 (2021), https://doi.org/10.3390/en14041207.
[40] L. Zecchi, G. Sandrini, M. Gadola, D. Chindamo, Modeling of a hybrid fuel cell powertrain with power split logic for onboard energy management using a longitudinal dynamics simulation tool, Energies 15 (2022) 6228, https://doi.org/10.3390/en15176228.
[41] G. Sandrini, M. Gadola, D. Chindamo, L. Zecchi, Model of a hybrid electric vehicle equipped with solid oxide fuel cells powered by biomethane, Energies 16 (2023) 4918, https://doi.org/10.3390/en16134918.
[42] G. Sandrini, M. Gadola, D. Chindamo, P. Magri, Application of solid oxide fuel cells on hybrid electric vehicles operating in fleet, Transport. Res. Procedia 70 (2023) 20–27, https://doi.org/10.1016/j.trpro.2023.10.004.
[43] J. Guo, F. Jiang, A novel electric vehicle thermal management system based on cooling and heating of batteries by refrigerant, Energy Convers. Manag. 237 (2021) 114145, https://doi.org/10.1016/j.enconman.2021.114145.
[44] M. Sreekanth, M. Feroskhan, J. Daniel, N. Gobinath, Heat load estimation and thermodynamic analysis of the thermal management of an electric car, Mater. Today Proc. (2023), https://doi.org/10.1016/j.matpr.2023.01.280.
[45] VI-Grade, Off-line simulations. https://www.vi-grade.com/en/solutions/off-line_simulations/. (Accessed 14 November 2024).
[46] MathWorks, datasheet battery. https://it.mathworks.com/help/autoblks/ref/datasheetbattery.html?searchHighlight=DATASHEET%20BATTERY&s_tid=srchtitle_support_results_1_DATASHEET%20BATTERY. (Accessed 31 October 2023).
[47] W. Cao, C. Zhao, Y. Wang, T. Dong, F. Jiang, Thermal modeling of full-size-scale cylindrical battery pack cooled by channeled liquid flow, Int. J. Heat Mass Tran. 138 (2019) 1178–1187, https://doi.org/10.1016/j.ijheatmasstransfer.2019.04.137.

[48] Samsung SDI Co, Ltd. Cell business division, specification of product for lithium-ion rechargeable cell. https://www.tme.eu/Document/bdf3bec3bd9898cb175128fb3dc18769/ACCU-INR18650-29E.pdf, 2014. (Accessed 31 October 2023).
[49] S.M.R. Islam, S.-Y. Park, B. Balasingam, Unification of internal resistance estimation methods for Li-ion batteries using hysteresis-free equivalent circuit models, Batteries 6 (2020) 32, https://doi.org/10.3390/batteries6020032.
[50] L. Chen, M. Zhang, Y. Ding, S. Wu, Y. Li, G. Liang, H. Li, H. Pan, Estimation the internal resistance of lithium-ion-battery using a multi-factor dynamic internal resistance model with an error compensation strategy, Energy Rep. 7 (2021) 3050–3059, https://doi.org/10.1016/j.egyr.2021.05.027.
[51] Argonne National Laboratory, BatPaC, Battery manufacturing cost estimation. https://www.anl.gov/partnerships/batpac-battery-manufacturing-cost-estimation. (Accessed 25 February 2022).
[52] M. Lu, X. Zhang, J. Ji, X. Xu, Y. Zhang, Research progress on power battery cooling technology for electric vehicles, J. Energy Storage 27 (2020) 101155, https://doi.org/10.1016/j.est.2019.101155.
[53] PubChem, stearyl alcohol. https://pubchem.ncbi.nlm.nih.gov/compound/Stearyl-Alcohol. (Accessed 4 December 2023).
[54] L. Bushi, T. Skszek, D. Wagner, MMLV: life cycle assessment. https://doi.org/10.4271/2015-01-1616, 2015.
[55] O. Ahmadzadeh, R. Rodriguez, J. Getz, S. Panneerselvam, D. Soudbakhsh, The impact of lightweighting and battery technologies on the sustainability of electric vehicles: a comprehensive life cycle assessment, Environ. Impact Assess. Rev. 110 (2025) 107668, https://doi.org/10.1016/j.eiar.2024.107668.
[56] Z. Songlin, L. XI, Lightweight design of vehicle components based on strengthening effects of low-amplitude loads below fatigue limit, Fatig. Fract. Eng. Mater. Struct. 35 (2012) 269–277, https://doi.org/10.1111/j.1460-2695.2011.01615.x.
[57] H.-W. Raedt, F. Wilke, C.-S. Ernst, Lightweight forging initiative phase II: lightweight design potential for a light commercial vehicle, ATZ Worldwide 118 (2016) 48–53, https://doi.org/10.1007/s38311-015-0110-1.